

Supplementary information

Additional notes and results for “Coupling mixture designs, high-throughput experiments and machine learning for accelerated exploration of multinary systems”

Elise GAREL, Jean-Luc PAROUTY, Hugo VAN LANDEGHEM, Marc VERDIER, Florence ROBAUT, Stéphane COINDEAU, Raphaël BOICHOT

Univ. Grenoble Alpes, CNRS, Grenoble INP, SIMAP, 38000 Grenoble, France

Table des matières

<i>Supplementary Notes</i>	4
Supplementary Note 1: Linear gradients and planar gradients in N-dimensions space	4
Supplementary Note 2: Set of gradients and target list	11
Supplementary Note 3: Nano-indentation experimental error – Surface roughness and indent tilting	12
Supplementary Note 4: Representation of an N-element composition space and screening	16
Supplementary Note 5: Model error distribution	20
Supplementary Note 6: Machine Learning models	22
Supplementary Note 7: Binaries validation set	28
<i>Supplementary Figures</i>	30
<i>Supplementary Tables</i>	48

Supplementary Figure 1 : Simplex Centroid mixture design in a ternary	4
Supplementary Figure 2: For 5-components system, size distribution of gradient sets randomly selected, after 2000 brute-force runs and an example of a gradient set composed of 13 gradients (the minimal number found), passing at least once by each point of Simplex-Centroid Mixture Design . The absence of solution with 18 gradients for 5 elements is unexplained but repeatable.....	9
Supplementary Figure 3: Matlab brute force algorithm principle (Gitlab repository)	10
Supplementary Figure 4 : AFM image of $Zr_{7.6}Nb_{87.2}Ti_{5.1}$ (error signal left, height right)	12
Supplementary Figure 5 : AFM image for $Zr_{8.3}Mo_{29}Cr_{62.7}$ with an indent imprint (error signal left, height right)	12
Supplementary Figure 6 : AFM image for $Zr_{19.2}Mo_{25.9}Cr_{54.9}$ (error signal left, height right)	12
Supplementary Figure 7 : The Berkovitch tip used to generate the hardness/Young’s modulus dataset	13
Supplementary Figure 8 : d and z measured along the most prominent vertex.....	13
Supplementary Figure 9 : Principle of calculation for the tip/surface inclination angle with a Berkovitch tip.....	14
Supplementary Figure 10: Nano-indentation curves of three different areas. The values kept were taken at 350 nm	15
Supplementary Figure 11: Figure from Miracle et Senkov, « A critical review of high entropy alloys and related concepts » ⁶ showing different representation of multinaries composition space. a) proposition, an isometric projection, has a major flaw for the method developed here as DE binary,	

ABC, ADE, BDE and CDE ternaries, all quaternary and quinaries are overlapping. This mean this representation is not able to show properly the center of the composition space, which is the main concern for multinaries. The b) and c) propositions do not really facilitate the visualization of an interesting domain.	16
Supplementary Figure 12: Representations of composition points in a quinary proposed by Banko et al: 2D 5-cell (A), 3D 5-cell (B), quasi-quaternary (C).	16
Supplementary Figure 13: Simplex-Centroid Mixture Design points in 2D 5-cell representation with an example of 7 point alignment in the 2D projection that does not exists in a 4D space.	17
Supplementary Figure 14: Delaunay triangulation for 5 to 10 element composition space. Vertices coordinates are randomly generated from normal distribution	18
Supplementary Figure 15: a) Simplex centroid mixture design points in a senary represented by a Delaunay triangulation of vertices randomly generated from a normal distribution: we observe no overlapping of the composition points b) and c) two views of the same composition	
Nb ₁₀ Ti ₂₀ Zr ₃₀ Cr ₁₅ Mo ₁₀ Al ₅ in the composition space	19
Supplementary Figure 16 : Standard error estimate for simulated properties calculated from our experimental dataset compositions.....	20
Supplementary Figure 17: Prediction-experience deviation along the binary gradients	28
Supplementary Figure 18: Predicted phase class vs experimental XRD phase class for the three binaries	29
Supplementary Figure 19: Sample map of a quaternary A-B-C-D screened with four cathodes and of a quinary A-B-C-D-E screened with five cathodes. The map corresponds to a projection of the 3D and 4D composition spaces in 2D leading to an overlapping of some mixtures. In the quaternary, AC and BD mixtures cannot be obtained; in both mixtures, ternary cannot be obtained either. Using more than three cathodes is then inefficient to guarantee a regular screening of the composition space on a 2D substrate.....	30
Supplementary Figure 20 : EBSD maps for 4 compositions, as Inverse Pole figure, Confidence Index map and Image Quality map, from amorphous to almost single crystal.	30
Supplementary Figure 21: XRD diffraction patterns for 4 compositions, from amorphous to almost single crystal.....	31
Supplementary Figure 22: SEM image of Zr ₉ Nb ₄₀ Mo ₁₇ Ti ₁₃ Cr ₂₁ and corresponding EBSD map. Due to substrate bias, ion bombarding has locally etched the surface. The surface appears amorphous on the EBSD map, with very badly defined orientations. The crystalline zones are on the contrary corresponding to etched zones. XRD shows diffraction peaks for this composition.	31
Supplementary Figure 23: Experimental value of elastic modulus	32
Supplementary Figure 24: Experimental value of hardness	32
Supplementary Figure 25 : EBSD experimental phase class	32
Supplementary Figure 26: XRD experimental phase class	32
Supplementary Figure 27 : Coefficients of quartic multiple regression on Young Modulus. Coefficient C _i corresponding to an interaction terms of degree n are plotted as (C _i) ^{1/n} . Bar color depends on the p-value of the hypothesis H ₀ that the coefficients C _i are equal to zero, meaning that the associated parameter or interaction has no influence on the response. Coefficients with p-value = 0 (significant) are plotted in green, 0 <p-value< 0.05 are plotted in blue, p-value > 0.05 (non-significant) are plotted in white.....	33
Supplementary Figure 28: Coefficients of quartic multiple regression on Hardness. Coefficient C _i corresponding to an interaction terms of degree n are plotted as (C _i) ^{1/n} . Bar color depend on the p-value of the hypothesis H ₀ that the coefficients C _i are equal to zero, meaning that the associated parameter or interaction has no influence on the response. Coefficients with p-value = 0 (significant) are plotted in green, 0 <p-value< 0.05 are plotted in blue, p-value > 0.05 (non-significant) are plotted in white	33

Supplementary Figure 29: Regressions between predicted and expected values on test sets of elastic modulus, and MAE metric distribution for different Machine Learning models, with "Raw data" datasets	34
Supplementary Figure 30: Regressions between predicted and expected values on test sets of elastic modulus, and MAE metric distribution for different Machine Learning models, with "Threshold data" dataset.....	35
Supplementary Figure 31: Regressions between predicted and expected values on test sets of elastic modulus, and MAE metric distribution for different Machine Learning models, with "Statistically processed data" dataset.....	36
Supplementary Figure 32: Regressions between predicted and expected values on test sets of elastic modulus, and MAE metric distribution for different Machine Learning models, with "Averaged data" dataset.....	37
Supplementary Figure 33: Regressions between predicted and expected values on test sets of hardness, and MAE metric distribution for different Machine Learning models, with "Raw data" dataset	38
Supplementary Figure 34 : Regressions between predicted and expected values on test sets of hardness, and MAE metric distribution for different Machine Learning models, with "Threshold data" dataset.....	39
Supplementary Figure 35 : Regressions between predicted and expected values on test sets of hardness, and MAE metric distribution for different Machine Learning models, with "Statistically processed data" dataset.....	40
Supplementary Figure 36 : Regressions between predicted and expected values on test sets of hardness, and MAE metric distribution for different Machine Learning models, with "Averaged data" dataset.....	41
Supplementary Figure 37 : Regressions between predicted and expected values on test sets of EBSD Confidence Index (CI), and MAE metric distribution for different Machine Learning models, with "Averaged data" dataset	42
Supplementary Figure 38 : Regressions between predicted and expected values on test sets of EBSD Image Quality (IQ), and MAE metric distribution for different Machine Learning models, with "Averaged data" dataset	43
Supplementary Figure 39 : Confusion matrix between predicted and expected values on test sets of EBSD Confidence Index (CI), and accuracy metric distribution for different Machine Learning models, with "Averaged data" dataset.....	44
Supplementary Figure 40 : Confusion matrix between predicted and expected values on test sets of XRD phase classes, and accuracy metric distribution for different Machine Learning models, with "XRD classes" dataset	45
Supplementary Figure 41 : Precicted phases of the quinary system, with 2%at composition step for each element	46
Supplementary Figure 42 : Pareto-optimal composition obtained in amorphous (a) and crystalline (b) domains from Random Forest predictions	46
Supplementary Figure 43: Pareto-optimal compositions predicted by Random Forest models trained with intial dataset without outliers iteratively completed with binaries.....	47

Supplementary Notes

Supplementary Note 1: Linear gradients and planar gradients in N -dimensions space

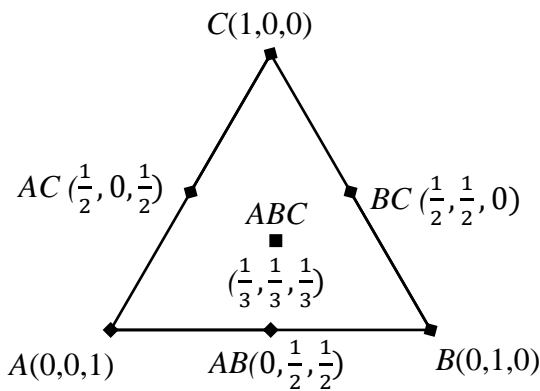
An N -element composition space is represented in an $(N-1)$ -simplex, which consists in the convex hull of N points in general position, or to the extension in $(N-1)$ dimensions of a triangle. Composition space of 2 elements is represented by a 1D segment along which the composition of each element evolves between 0% and 100%; a 3-element composition is represented by an equilateral 2D triangle, a 4-element composition space by a 3D tetrahedron, a 5-element space by a 4D hyper-tetrahedron.

A regular screening of such spaces was proposed by Scheffé and al¹, using a Simplex Centroid mixture design, that consists in studying certain discrete points corresponding to all pure elements and equimolar or equimassic mixtures (binaries, ternaries, etc). From now on, binaries can also be designated as 2nd order mixtures, ternaries by 3rd order mixtures and so on.

The coordinates of such compositions in N dimensions can be written as permutations of the n-tuples:

$$\begin{aligned}
 & n - aries \left(\frac{1}{n}, \frac{1}{n}, \dots, \frac{1}{n} \right) \\
 & (n-1) - aries \left(\frac{1}{n-1}, \frac{1}{n-1}, \dots, \frac{1}{n-1}, 0 \right) \dots \\
 & q - naries \left(\frac{1}{q}, \frac{1}{q}, \dots, \frac{1}{q}, 0, \dots, 0 \right) \\
 & \quad \dots \\
 & binaries \left(\frac{1}{2}, \frac{1}{2}, 0, \dots, 0 \right) \\
 & unaries (1, 0, 0, \dots, 0)
 \end{aligned}$$

An example of a Simplex Centroid for a ternary space is given hereafter:



Supplementary Figure 1 : Simplex Centroid mixture design in a ternary

Using a combinatorial approach, one will not only study these discrete points but a continuum of compositions passing through several points of the mixture design. Linear gradients or planar gradients can be studied on a 2D sample, without any distortion that the projection of a higher dimension space on the sample would otherwise cause.

A single linear gradient can go through up to three points of the mixture design. A single planar gradient can contain up to seven points of the mixture design, as it can be easily seen on the Simplex Centroid mixture design with only three elements on the Supplementary Figure 1.

In the following, the alignment condition of three points will be mathematically proved and the number of possible linear gradients in an N -element composition space will be determined. The same approach will be developed for planar gradients.

Linear gradients between three points of the mixture design: alignment conditions.

The mixture design points correspond to barycenters and can thus be identified with their barycentric coordinates. Notice that the barycentric coordinates give the compositions of the corresponding mixtures.

eg 1: In a 2-element composition space, $A(1,0)$ and $B(0,1)$ are the two pure elements and the binary AB , their barycenter, is written $AB\left(\frac{1}{2}, \frac{1}{2}\right) = \left(A, \frac{1}{2}\right), \left(B, \frac{1}{2}\right) = \frac{1}{2}A + \frac{1}{2}B$ meaning that point A and point B have the same contribution to the AB binary.

eg 2: In a 3-element composition space, $A(1,0,0), B(0,1,0), C(0,0,1)$ are the three pure elements and the binary AC , the barycenter of A and C is written $ABC\left(\frac{1}{2}, 0, \frac{1}{2}\right) = \left(A, \frac{1}{2}\right), \left(B, 0\right), \left(C, \frac{1}{2}\right) = \frac{1}{2}A + 0 \times B + \frac{1}{2}C$ meaning that point A and point C have the same contribution to the AC binary.

eg 3: In a 4-element composition space, $A(1,0,0,0), B(0,1,0,0), C(0,0,1,0), D(0,0,0,1)$ are the four pure elements and the ternary ABC , the barycenter of A, B and C is written $ABC\left(\frac{1}{3}, \frac{1}{3}, \frac{1}{3}, 0\right) = \left(A, \frac{1}{3}\right), \left(B, \frac{1}{3}\right), \left(C, \frac{1}{3}\right), \left(D, 0\right) = \frac{1}{3}A + \frac{1}{3}B + \frac{1}{3}C + 0.D$ meaning that point A , point B and point C have the same contribution to the ABC ternary.

Let O, P and Q three points of the mixture design of N elements $[X_1, X_2, X_3, \dots, X_N]$, of order o, p and q (comprised between 1 and n). Their coordinates are permutations of the following n -tuples:

$$\begin{aligned} O & \left(\underbrace{\frac{1}{o}, \frac{1}{o}, \frac{1}{o}, \dots, \frac{1}{o}}_{o \text{ terms}}, 0, 0, \dots, 0 \right) \#(1) \\ P & \left(\underbrace{\frac{1}{p}, \frac{1}{p}, \frac{1}{p}, \dots, \frac{1}{p}}_{p \text{ terms}}, 0, 0, \dots, 0 \right) \#(2) \\ Q & \left(\underbrace{\frac{1}{q}, \frac{1}{q}, \frac{1}{q}, \dots, \frac{1}{q}}_{q \text{ terms}}, 0, 0, \dots, 0 \right) \#(3) \end{aligned}$$

Thus, for all $i \in \llbracket 1, N \rrbracket$:

- X_i concentration of O , denoted by $x_{i,O}$, is equal to 0 or $\frac{1}{o}$,
- X_i concentration of P , denoted by $x_{i,P}$, is equal to 0 or $\frac{1}{p}$,
- X_i concentration of Q , denoted by $x_{i,Q}$, is equal to 0 or $\frac{1}{q}$.

We assume that O is aligned with P and Q and the three points are distinct. Without loss of generality, we can assume that O is in between P and Q . Then:

$$\exists(a, b) \in (\mathbb{R}^{*+})^2, O = aP + bQ \text{ with } a + b = 1.$$

Let $i \in \llbracket 1, N \rrbracket$, we have $x_{i,o} = ax_{i,p} + bx_{i,q}$.

$$\text{Thus, since } a, b > 0 \text{ we have: } x_{i,o} = \begin{cases} 0 & \text{if } x_{i,p} = x_{i,q} = 0, \\ \frac{a}{p} & \text{if } x_{i,p} = \frac{1}{p} \text{ and } x_{i,q} = 0, \\ \frac{b}{q} & \text{if } x_{i,p} = 0 \text{ and } x_{i,q} = \frac{1}{q}, \\ \frac{a}{p} + \frac{b}{q} & \text{if } x_{i,p} = \frac{1}{p} \text{ and } x_{i,q} = \frac{1}{q}. \end{cases}$$

Notice that as $a > 0$ and $b > 0$, if for some $i \in \llbracket 1, N \rrbracket$ $x_{i,o} = 0$ then $x_{i,p} = 0$ and $x_{i,q} = 0$, and conversely. Then P, Q have the same contributions from X_i , equal to 0.

Moreover: for all $i \in \llbracket 1, N \rrbracket$ such that $x_{i,o} \neq 0$, we have $x_{i,o} = ax_{i,p} + bx_{i,q}$ which implies

$$\frac{1}{o} = \frac{a}{p} \quad \text{or} \quad \frac{1}{o} = \frac{b}{q} \quad \text{or} \quad \frac{1}{o} = \frac{a}{p} + \frac{b}{q}.$$

Notice that last equation $\frac{a}{p} + \frac{b}{q} = \frac{1}{o}$ is not compatible with any of the two others: if

$$\frac{a}{p} = \frac{1}{o} = \frac{a}{p} + \frac{b}{q}$$

Then $a = b = 0$ and similarly for $\frac{b}{q} = \frac{1}{o} = \frac{a}{p} + \frac{b}{q}$.

Case n°1:

$$\frac{a}{p} + \frac{b}{q} = \frac{1}{o}$$

In this case, there are as much non zeros terms in P as in Q thus $p = q$ (see equations (2) and (3)), and P and Q have exactly the same barycentric coordinates. This case can be ignored.

Case n°2: As the previous equation is not verified, and as for all $i \in \llbracket 1, N \rrbracket$ such that $x_{i,p} \neq 0$ then $x_{i,q} = 0$ and for all $i \in \llbracket 1, N \rrbracket$ such that $x_{i,q} \neq 0$ then $x_{i,p} = 0$. Then P and Q have complementary compositions and since P and Q have at least one non zero coordinate we have:

$$\frac{1}{o} = \frac{a}{p} \quad \text{and} \quad \frac{1}{o} = \frac{b}{q}.$$

Then:

$$a = \frac{p}{o} \quad \text{and} \quad b = \frac{q}{o}.$$

Since $a = 1 - b$, $o = p + q$

As a conclusion, O , in between P and Q , is the higher order mixture, and P and Q have a complementary composition, meaning the contributions of X_i to P and the contribution of X_i to Q are complementary: these mixture have no common elements. Mixture order must verify $o = p + q$.

Now let P and Q be two distinct compositions. By what we prove previously, for P and Q to be aligned with another composition point of the mixture design, we need one of the following conditions:

1. P and Q do not have any component in common.
2. All components of Q are components of P (Q composition is strictly included in P composition).

3. All components of P are components of Q (P composition is strictly included in Q composition).

In the first case, the composition of the third point O is a sum of the two others, i.e. the equimolar mixture of all the components which appear in the compositions of P and Q. Then $o = p + q$ is verified.

The last two cases are symmetric, with $q < p$ in case 2 and $q > p$ in case 3. In both cases, the third point O corresponds to the complementary composition of the lower order mixture in the higher order one (e.g. O composition is the complementary of Q composition in P in the case 2). Thus $q = o + p$ in case 2, and $p = o + q$ in case 3.

Number of linear gradients in a N -element composition space passing by three points of Simplex Centroid Mixture Design

- The number of p -element mixtures in an N -element composition space is $\binom{N}{p}$. As the q -nary should have a complementary composition, this leaves $N-p$ elements.
- Then, for all o in $[2, N]$ and for all p in $[1, o - 1]$, choosing a gradient or alignment going through two mixtures of order p and q with compositions complementary to a mixture of order o is numbered as:

$$\binom{N}{p} \binom{N-p}{q} = \binom{N}{p} \binom{N-p}{o-p}.$$

- For each alignment there are $2! = 2$ possible arrangements
eg: A – ABC – BC and BC – ABC – A are two arrangements of the same gradient
- By summing, the total number of gradients is:

$$S_{gradients} = \frac{1}{2!} \sum_{o=2}^N \sum_{p=1}^{o-1} \binom{N}{p} \binom{N-p}{o-p}. \#(6)$$

With a rearrangement of the binomial coefficients:

$$\binom{N}{p} \binom{N-p}{o-p} = \frac{N!}{(N-p)! p!} \frac{(N-p)!}{(o-p)! (N-p-o+p)!} = \frac{N!}{p! (o-p)! (N-o)!},$$

a multinomial coefficient can be recognized:

$$\frac{N!}{p! (o-p)! (N-o)!} = \binom{N}{p, o-p, N-o} = \binom{N}{p, q, r}.$$

with $q = o - p$, $r = N - o$ and $p + q + r = N$

and $0 \leq r \leq N - 2$, $1 \leq p \leq N - 1$ and $1 \leq q \leq N - 1$.

Equation (6) can be re-written:

$$S_{gradients} = \frac{1}{2} \left(\sum_{\substack{p+q+r=N \\ p \geq 1 \\ q \geq 1}} \binom{N}{p, q, r} - \sum_{\substack{q+r=N \\ q \geq 1}} \binom{N}{0, q, r} - \sum_{\substack{p+r=N \\ p \geq 1}} \binom{N}{p, 0, r} + \binom{N}{0, 0, N} \right)$$

$$S_{gradients} = \frac{1}{2} (3^N - 2^{N+1} + 1)$$

For an N -element composition space, the total number of gradients going through three points of the Simplex Centroid mixture design is $S_{gradients} = \frac{1}{2}(3^N - 2^{N+1} + 1)$. It is the total number of samples that can be fabricated to screen the composition space homogeneously.

Number of planar gradients in a N -element composition space encompassing seven points of a Simplex Centroid Mixture Design

The section of a simplex that passes through points of mixture design is a triangle. Its edges are the previously identified gradients, with one common end. The gradient center is also a point of the mixture design; thus, the plane passes by six points of the mixture design.

The ends of each gradient correspond to complementary compositions, so the vertices of the triangle have complementary compositions in pairs. Each alignment center has a complementary composition to the opposite vertex, so the medians of the triangle are also identified gradients.

The center of gravity of the triangle is therefore also a point of the mixture design.

A planar gradient can pass by seven points of the mixture design.

- To count all possible planar gradients passing by seven points of the mixture design, one may choose a p -nary, a q -nary and o -nary that form a triangle (P , Q and O are no more aligned). With complementary conditions previously highlighted, the gravity center of the plane is of order $r = o + p = p + q = q + o$ and $r \in [3, N]$.
- There are $3! = 6$ arrangements per planes.
- The total number of planes is then a sum of:

$$\begin{aligned} \binom{N}{p} \binom{N-p}{q} \binom{N-p-q}{o} &= \frac{N!}{(N-p)! p!} \frac{(N-p)!}{q! (N-p-q)!} \frac{(N-p-q)!}{o! (N-p-q-o)!} \\ &= \frac{N!}{p! q! o! (N-p-q-o)!} \\ &= \binom{N}{p, q, o, r} \end{aligned}$$

With $r = N - p - q - o$, $1 \leq p \leq N - 2$, $1 \leq q \leq N - 2$, $1 \leq o \leq N - 2$. By summing this multinomial coefficients:

$$\begin{aligned} S_{planes} &= \frac{1}{3!} \left(\sum_{p+q+o+r=N} \binom{N}{p, q, o, r} - \sum_{q+o+r=N} \binom{N}{0, q, o, r} - \sum_{p+o+r=N} \binom{N}{p, 0, o, r} \right. \\ &\quad \left. - \sum_{p+q+r=N} \binom{N}{p, q, 0, r} + \sum_{o+r=N} \binom{N}{0, 0, o, r} + \sum_{p+r=N} \binom{N}{0, q, 0, r} - \binom{N}{0, 0, 0, N} \right) \end{aligned}$$

$$S_{planes} = \frac{1}{6} (4^N - 3^{N+1} + 3 \cdot 2^N - 1).$$

For an N -element composition space, the total number of planar gradients passing by seven points of the Simplex Centroid mixture design is $S_{planes} = \frac{1}{6}(4^N - 3^{N+1} - 3 \cdot 2^N - 1)$. It is

the total number of samples that can be fabricated to screen the composition space homogeneously.

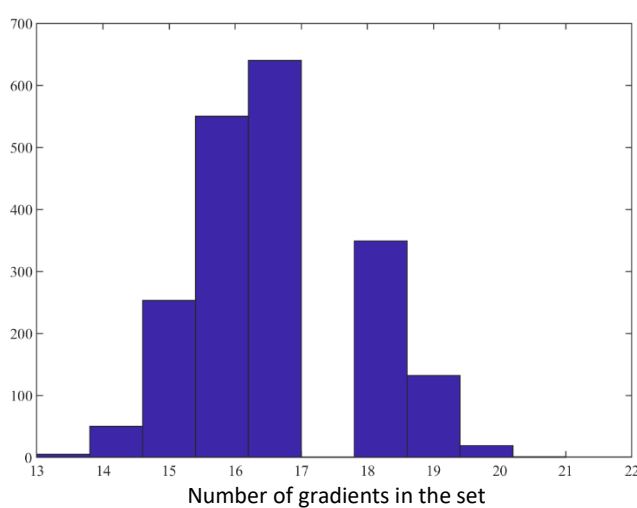
The total number of planar and linear gradients is computed for 3 to 7 elements. These sets of gradients can pass several times through the same composition point, hence it exists a minimum set of gradients that passes at least once through each point. This minimum number of gradients was computed by brute-force for 3 to 7.

Supplementary Table 1 : Number of possible linear and planar gradients passing by aligned mixture design points in N-element composition space for a Simplex Centroid Design.

Number of elements	3	4	5	6	7
Number of possible 1D linear gradients	6	25	90	301	966
Number of possible 2D planar gradients	1	10	65	350	1701

Supplementary Table 2 : Minimum number of linear and planar gradients to explore at least once each points of the Simplex Centroid mixture design, computed by brute-force

Number of elements	3	4	5	6	7
Lowest number of 1D linear gradients for complete screening	3	5	13	30	68
Lowest number of 2D planar gradients for complete screening	1	3	7	17	38



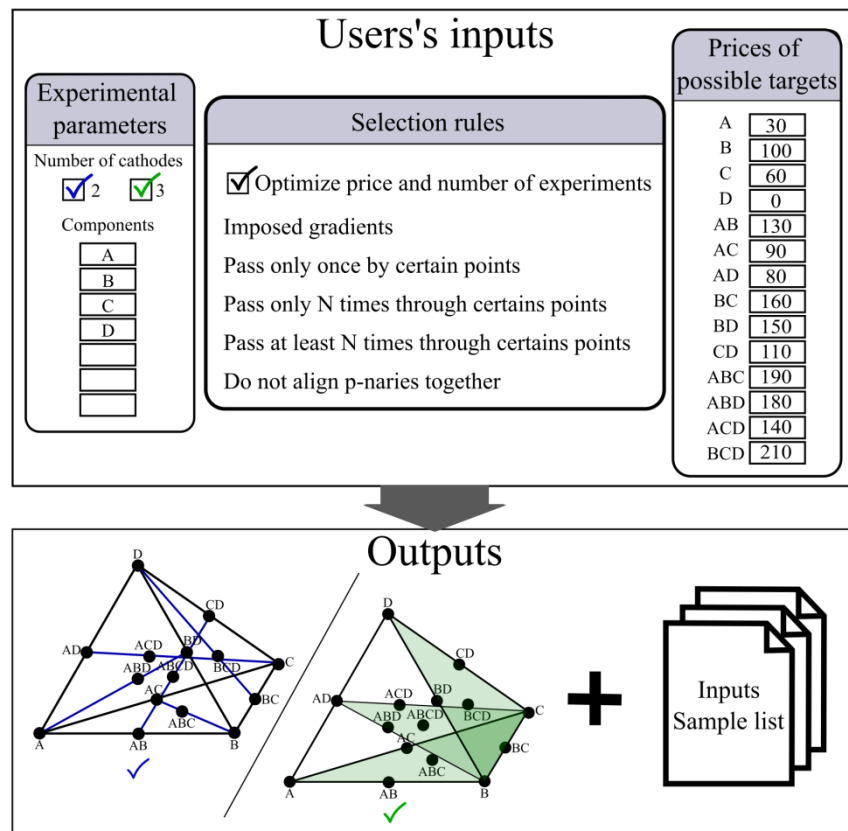
Example of a gradient set of size 13

Cr – NbTiCr – NbTi
 NbZr – NbTiZrCrMo – TiCrMo
 NbCr – NbTiZrCrMo – TiZrMo
 Ti – NbTiMo – NbMo
 TiZr – TiZrCrMo – CrMo
 NbMo – NbTiCrMo – TiCr
 TiMo – NbTiZrCrMo – NbZrCr
 Mo – ZrCrMo – ZrCr
 NbTi – NbTiZrMo – ZrMo
 Cr – NbTiZrCr – NbTiZr
 Nb – NbZrMo – ZrMo
 Zr – NbZrCrMo – NbCrMo

Supplementary Figure 2: For 5-components system, size distribution of gradient sets randomly selected, after 2000 brute-force runs and an example of a gradient set composed of 13 gradients (the minimal number found), passing at least once by each point of Simplex-Centroid Mixture Design . The absence of solution with 18 gradients for 5 elements is unexplained but repeatable.

Although it is possible to select a set of gradients oneself, an automated selection has been implemented in a Matlab interface. It can be particularly useful in the case of a very large number of possible gradients: indeed, choosing an optimal set of gradients passing at least once through each point of the mixture plane can be tedious. This implementation is particularly adapted to the elaboration method used in this study, the magnetron cathodic sputtering. Two cathodes allow the sputtering of two different targets, and thus the realization of linear gradients, while three cathodes allow the realization of planar gradients.

The interface was made to take into account some constraints imposed by the user. The interface principle is summed up in Supplementary Figure 3.



Supplementary Figure 3: Matlab brute force algorithm principle ([Gitlab repository](#))

Supplementary Note 2: Set of gradients and target list

The planned set of twenty gradients was chosen as:

- 1 NbTi — NbTiCrMo — CrMo
- 2 NbZr — NbZrCrMo — CrMo
- 3 TiZr — TiZrCrMo — CrMo
- 4 TiZr — NbTiZrCr — NbCr
- 5 TiZr — NbTiZrMo — NbMo
- 6 Nb — NbTiZr — TiZr
- 7 Nb — NbTiZrCrMo — TiZrCrMo
- 8 Nb — NbTiMo — TiMo
- 9 Ti — TiZrCr — ZrCr
- 10 Ti — TiZrMo — ZrMo
- 11 Ti — NbTiZrCrMo — NbZrCrMo
- 12 Zr — NbZrCr — NbCr
- 13 Zr — ZrCrMo — CrMo
- 14 Zr — NbTiZrCrMo — NbTiCrMo
- 15 Cr — NbTiCr — NbTi
- 16 Cr — NbCrMo — NbMo
- 17 Cr — NbTiZrCrMo — NbTiZrMo
- 18 Mo — NbZrMo — NbZr
- 19 Mo — TiCrMo — TiCr
- 20 Mo — NbTiZrCrMo — NbTiZrCr

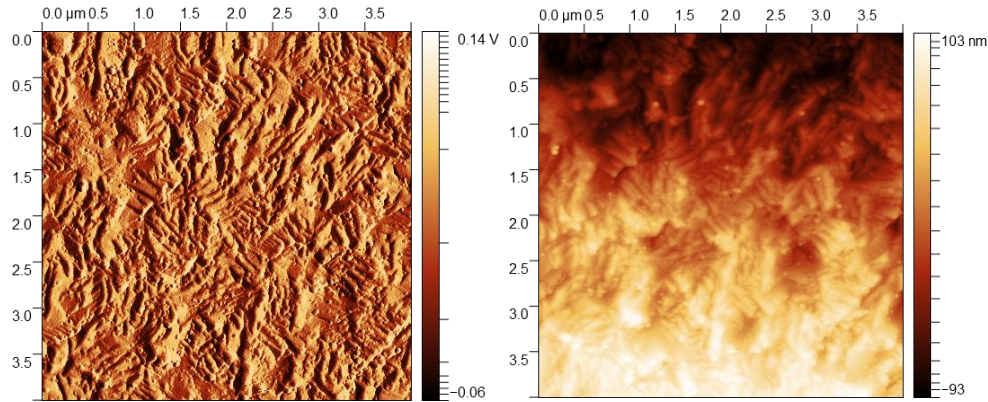
These require buying the following targets

- | | | |
|------|--------|------------|
| • Nb | • NbTi | • NbTiZrCr |
| • Ti | • NbZr | • NbTiZrMo |
| • Zr | • NbCr | • NbTiCrMo |
| • Cr | • NbMo | • NbZrCrMo |
| • Mo | • TiZr | • TiZrCrMo |
| | • TiMo | |
| | • TiCr | |
| | • ZrCr | |
| | • ZrMo | |
| | • CrMo | |

Supplementary Note 3: Nano-indentation experimental error – Surface roughness and indent tilting

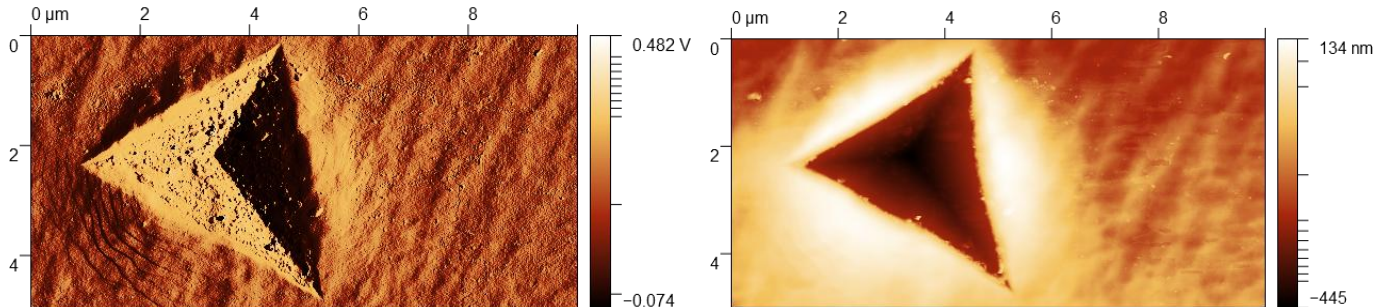
AFM was performed to assess the potential relationship between surface roughness and hardness value measured by nano-indentation. Sq stands for root mean square and Sa for arithmetic mean roughnesses.

Lowest hardness (3.9 GPa) is obtained for a crystalline phase, $Zr_{7.6}Nb_{87.2}Ti_{5.1}$. The roughness is measured on a $2 \mu\text{m}^2$ area: Sq = 15.21 nm and Sa = 3.39 nm.



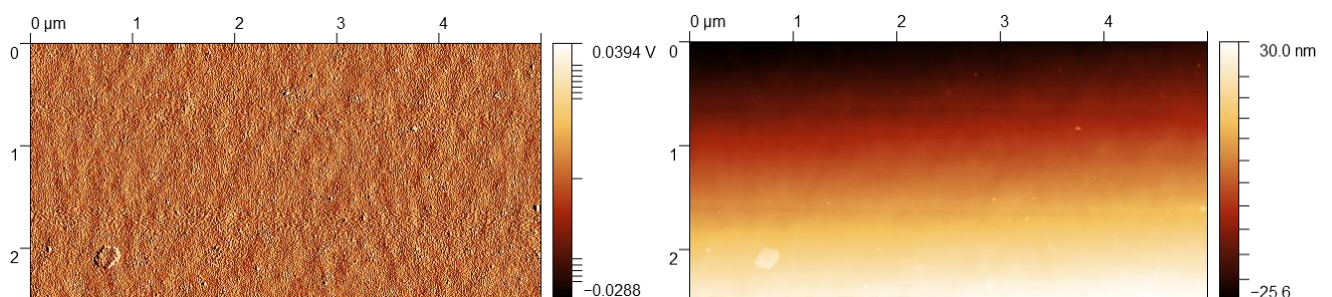
Supplementary Figure 4 : AFM image of $Zr_{7.6}Nb_{87.2}Ti_{5.1}$ (error signal left, height right)

Highest hardness (22 GPa) is obtained for a crystalline phase, $Zr_{8.3}Mo_{29}Cr_{62.7}$. We observe pile up of material around the imprint typical from ductile behaviour. The roughness is measured on a $2 \mu\text{m}^2$ area: Sq = 4.12 nm and Sa = 3.39 nm.



Supplementary Figure 5 : AFM image for $Zr_{8.3}Mo_{29}Cr_{62.7}$ with an indent imprint (error signal left, height right)

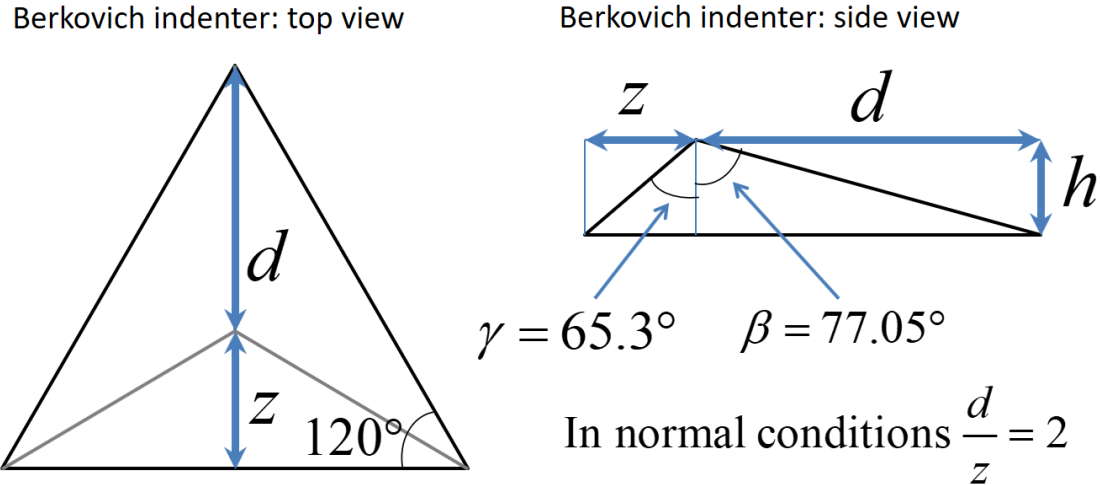
To complete, an amorphous zone with medium hardness (11 GPa), $Zr_{19.2}Mo_{25.9}Cr_{54.9}$, is also analyzed. The rugosity is measured on $2\mu\text{m}^2$ area: Sq= 12.39 nm and Sa= 10.72 nm.



Supplementary Figure 6 : AFM image for $Zr_{19.2}Mo_{25.9}Cr_{54.9}$ (error signal left, height right)

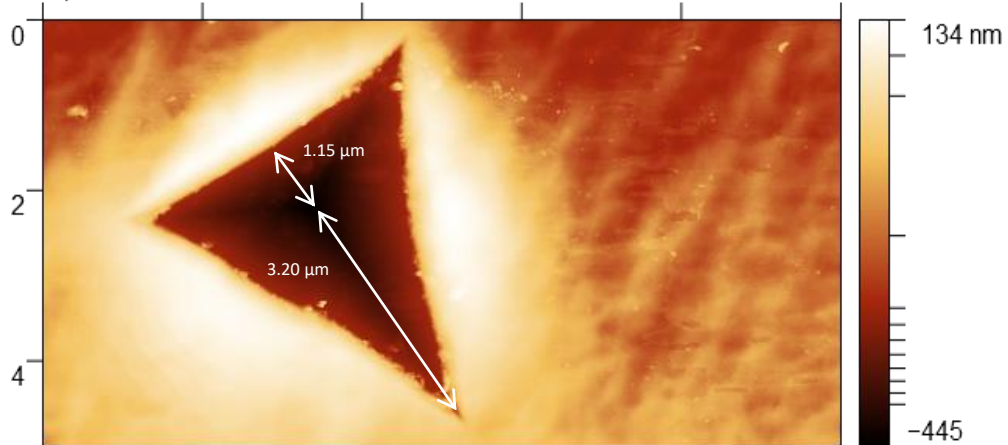
There is no clear correlation between roughness and hardness value. Overall, the roughness is negligible compared to the indent depth (350 nm).

On Supplementary Figure 4, we can observe that the indent trace is not symmetrical, due to a slight sample/tip tilt. This can induce an error on hardness measurement that can be evaluated. The typical Berkovitch tip we used is depicted in Supplementary Figure 6.



Supplementary Figure 7 : The Berkovitch tip used to generate the hardness/Young's modulus dataset

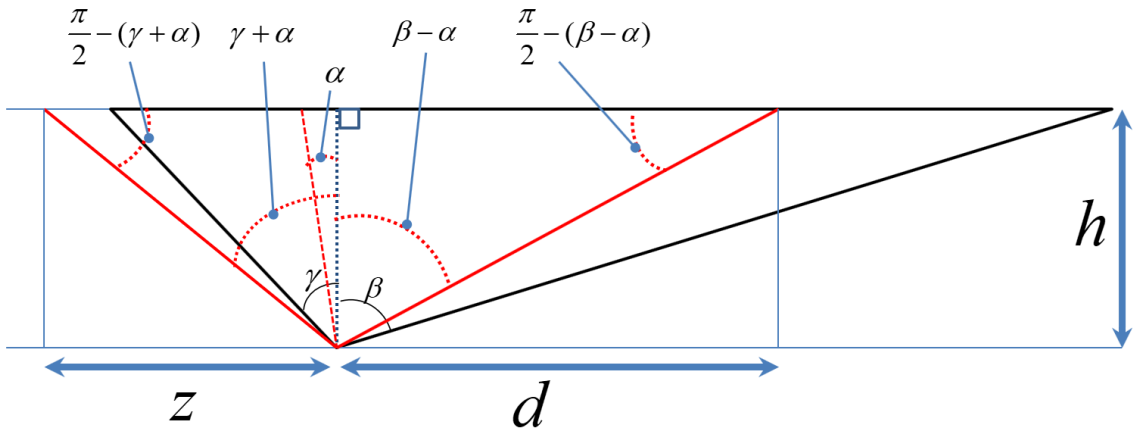
The indent trace must be a perfect equilateral triangle if the indentation is made perfectly perpendicular to the sample surface. May the sample surface not be perfectly flat (or inclined) or the tip arm not perfectly normal to the sample surface, the indent shape will become an irregular triangle. Supplementary Figure 7 shows the irregular indent depicted in Supplementary Figure 4 with the associated d and z measured along the most inclined direction, which corresponds to the principal tilt direction.



Supplementary Figure 8 : d and z measured along the most prominent vertex

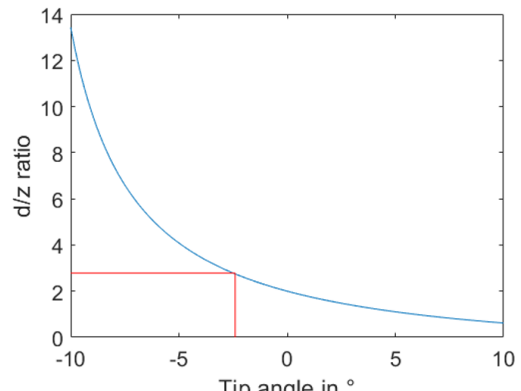
The inclination angle along each vertex can be recovered based on some basic trigonometry² (Supplementary Figure 8).

Berkovitch tip: case of an inclined indentation with angle α



$$\frac{d}{z} = \frac{\tan\left(\frac{\pi}{2} - (\gamma + \alpha)\right)}{\tan\left(\frac{\pi}{2} - (\beta - \alpha)\right)}$$

$$\frac{d}{z} = \frac{3.20}{1.15} = 2.78 \rightarrow \alpha = -2.4^\circ$$



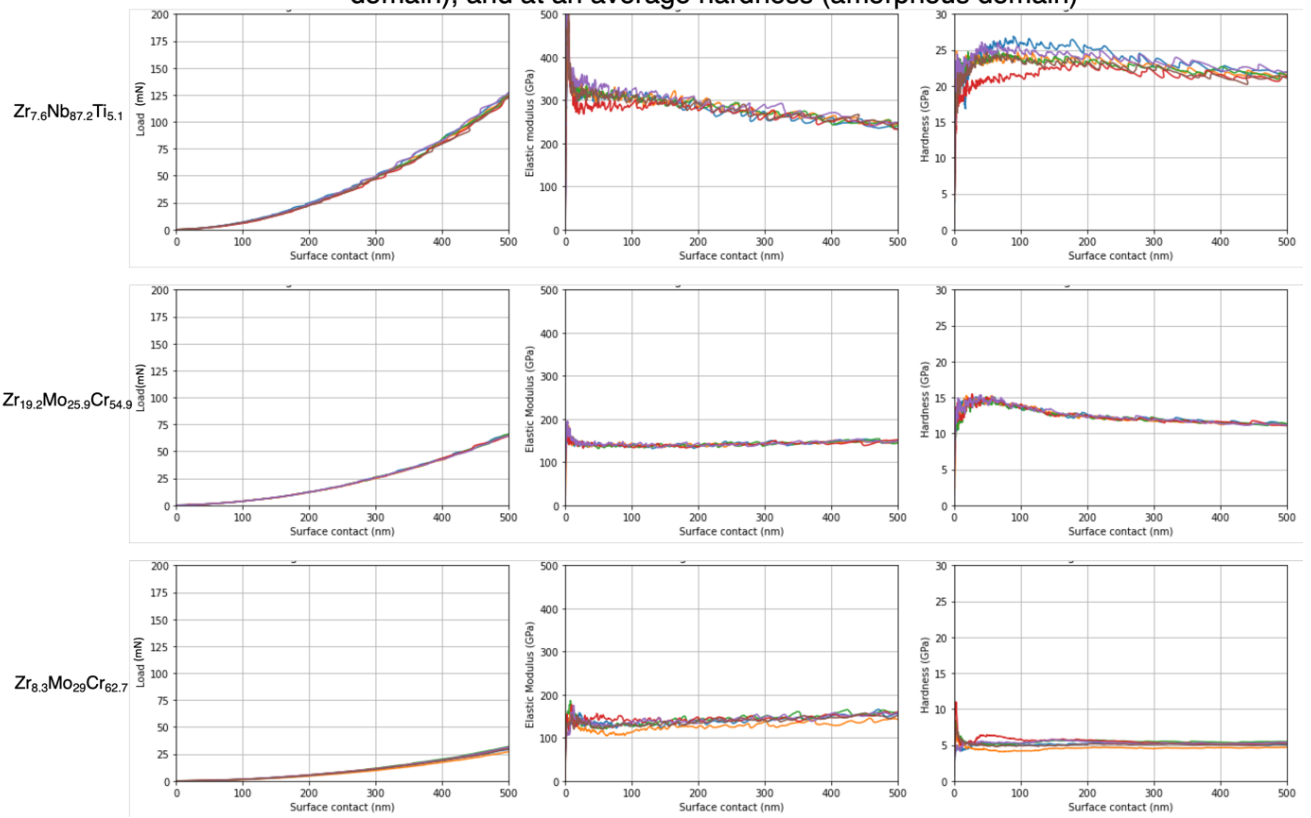
Supplementary Figure 9 : Principle of calculation for the tip/surface inclination angle with a Berkovitch tip.

In the case depicted in Supplementary Figure 7, with the formula of figure 8, we found that the maximum deviation angle during this nano-indentation trial is less than 2.5° (in absolute value). Instrumented indentation carried out with sharp tip geometries (akin to a cone) have the main advantage to be quite insensitive to small tip/sample tilt. This has been evaluated thoroughly in two publications^{3,4}, and it indicates a less than 3% error in Young modulus and Hardness evaluation for our tilt. This error is typically less than the experimental error due to variability of properties measured for one alloy composition.

Such a deviation cannot come from the sample surface (substrate being epi-ready sapphire and deposit being overall the same thickness on the sample), the deviation comes probably from the sample holder and must be the same for every sample. This implies that the error is constant throughout all tests. The absolute value of mechanical properties may be shifted but the detected tilt has no effect on the relative variations of properties within the full compositions set.

For information we give the nano-indentation curves corresponding to the area presented above in Supplementary Figure 10.

Nanoindentation curves for three compositions: at highest and lowest hardness (crystalline domain), and at an average hardness (amorphous domain)



Supplementary Figure 10: Nano-indentation curves of three different areas. The values kept were taken at 350 nm

Supplementary Note 4: Representation of an N-element composition space and screening

In their review of 2017, Senkov and Miracle⁶ show different ways to represent an N-elements composition space in an (N-1) spatial dimensions (for N higher than 4), for T and P constant.

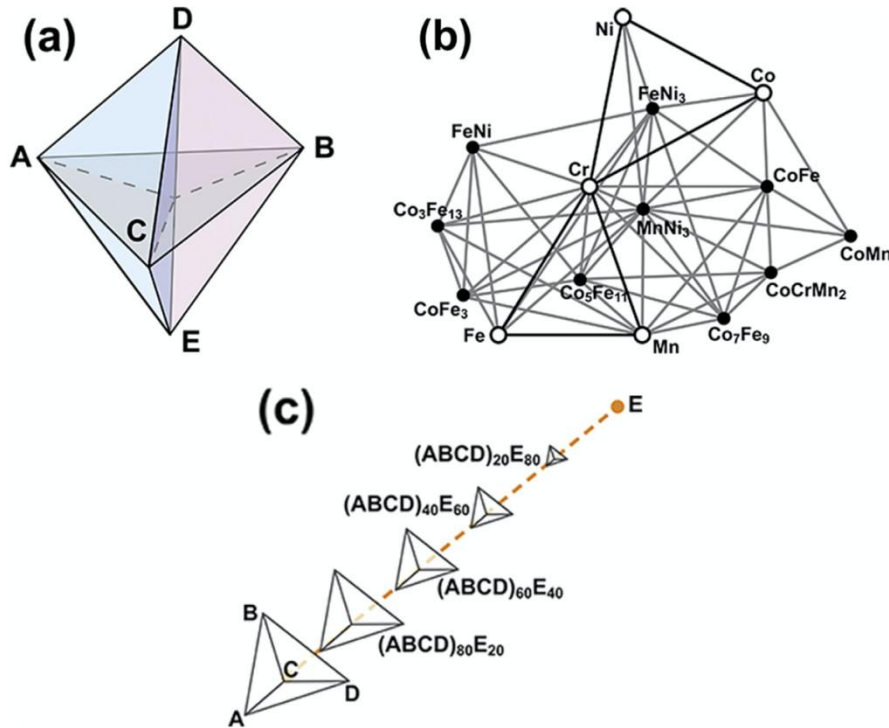
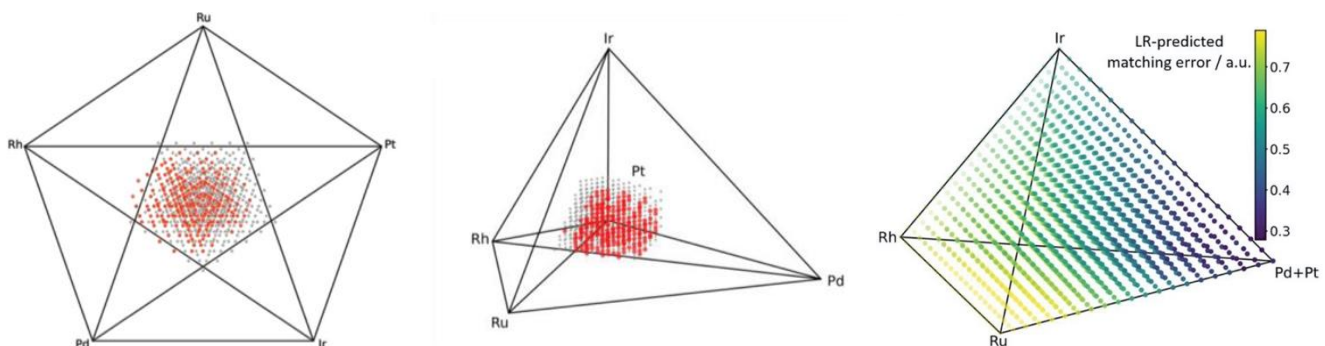


Fig. 1. Visual devices to illustrate 4D phase space in 2D. See text for descriptions.

Supplementary Figure 11: Figure from Miracle et Senkov, « A critical review of high entropy alloys and related concepts »⁶ showing different representation of multinaries composition space. a) proposition, an isometric projection, has a major flaw for the method developed here as DE binary, ABC, ADE, BDE and CDE ternaries, all quaternary and quinaries are overlapping. This mean this representation is not able to show properly the center of the composition space, which is the main concern for multinaries. The b) and c) propositions do not really facilitate the visualization of an interesting domain.

In 2019, Ludwig⁷ still highlights the need of an efficient “visualization of high-dimensional data”.

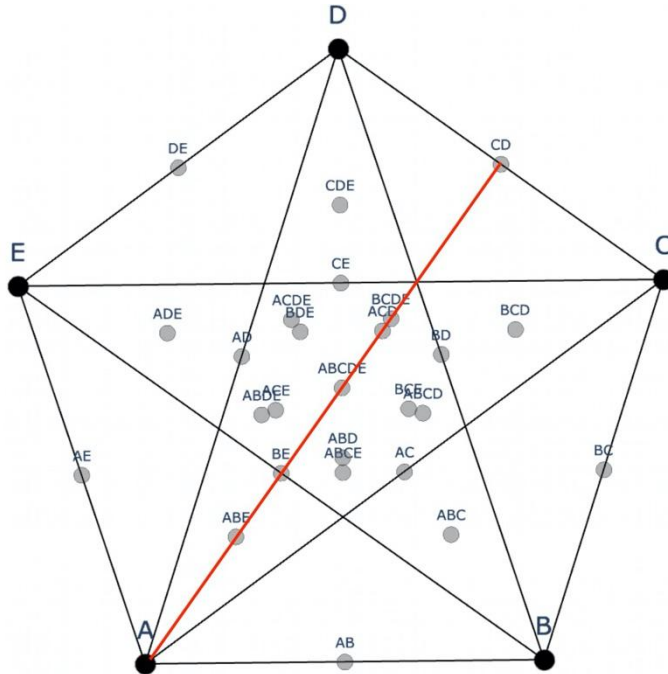
In 2022, Banko *et al* proposes three representations of a quinary system: a 2D, a quasi-quaternary representation for the same system and a 3D 5-cell representation (Supplementary Figure 10).



Supplementary Figure 12: Representations of composition points in a quinary proposed by Banko et al: 2D 5-cell (A), 3D 5-cell (B), quasi-quaternary (C).

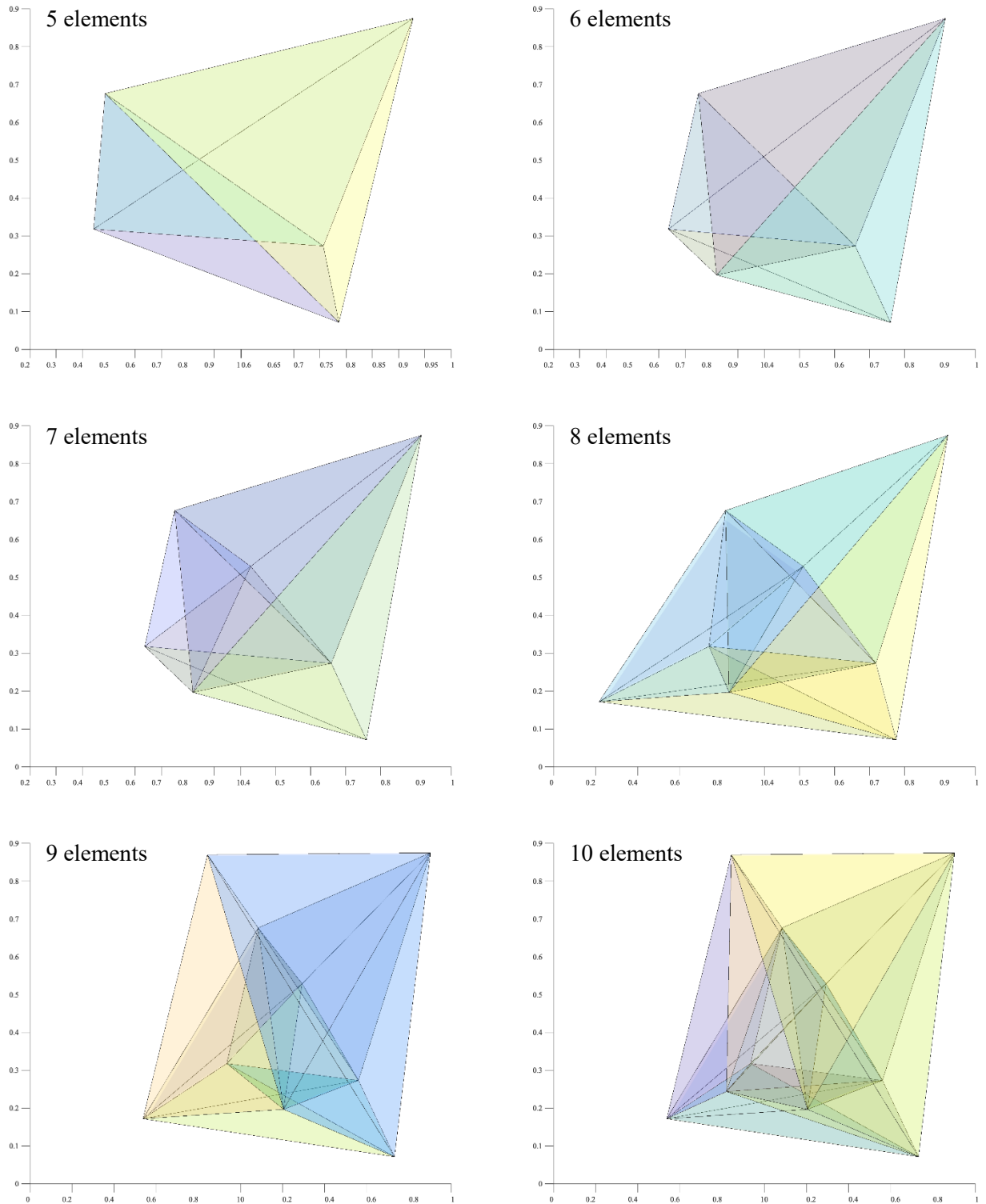
2D cell and quasi-quaternary representations have respectively two flaws:

- There is no clear separation of the SCD points, and some SCD points seem aligned while these alignments do not exist in the real space (see Supplementary Figure 11 for the 2D 5-cell case)
- Fixing a composition in the degrees of freedom is the opposite of mixture design principle.



Supplementary Figure 13: Simplex-Centroid Mixture Design points in 2D 5-cell representation with an example of 7 point alignment in the 2D projection that does not exists in a 4D space.

What is proposed in this paper is closer to the 3D 5-cell representation. It is based on a 3D Delaunay triangulation of N points. The points coordinates are a random sample from the standard uniform distribution. Delaunay triangulation in 3D will triangulate all these points (with a specific property: none of the N points are inside the circumsphere of any of the tetrahedra. The obtained tetrahedra are interconnected through their faces⁸). The Delaunay triangulation gives the convex hull of the N points⁹, ie a (N-1) simplex (see Supplementary Figure 12).



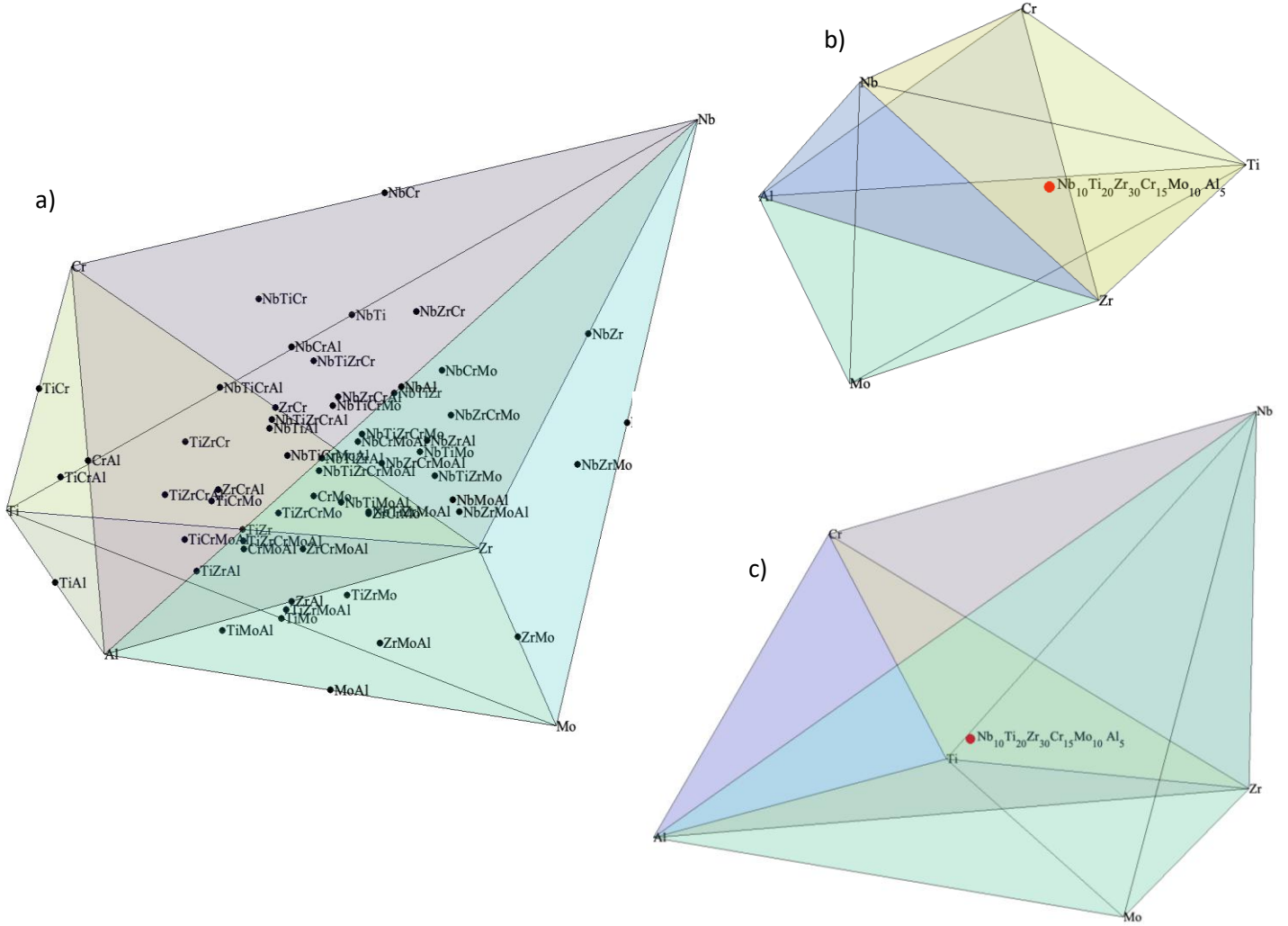
The obtained simplex is not a regular simplex as material experts are used to, but it allows to see correctly the center of the space without any overlapping of the mixture design points. The representation of compositions is very easy using barycentric coordinates. It can be noted that previous

demonstration of alignments was a general one, meaning that linear gradients and planes are not distorted in these irregular simplexes.

eg: $\text{Nb}_{10}\text{Ti}_{20}\text{Zr}_{30}\text{Cr}_{15}\text{Mo}_{10}\text{Al}_5$ is represented by the point of coordinates

$$\begin{pmatrix} x \\ y \\ z \end{pmatrix} = \begin{pmatrix} 0.1x_{Nb} + 0.2x_{Ti} + 0.3x_{Zr} + 0.15x_{Cr} + 0.1x_{Mo} + 0.05x_{Al} \\ 0.1y_{Nb} + 0.2y_{Ti} + 0.3y_{Zr} + 0.15y_{Cr} + 0.1y_{Mo} + 0.05y_{Al} \\ 0.1z_{Nb} + 0.2z_{Ti} + 0.3z_{Zr} + 0.15z_{Cr} + 0.1z_{Mo} + 0.05z_{Al} \end{pmatrix}$$

Interactive plotting as proposed in Matlab or with Matplotlib library of python is an asset to improve the visualization.



Supplementary Figure 15: a) Simplex centroid mixture design points in a senary represented by a Delaunay triangulation of vertices randomly generated from a normal distribution: we observe no overlapping of the composition points b) and c) two views of the same composition $\text{Nb}_{10}\text{Ti}_{20}\text{Zr}_{30}\text{Cr}_{15}\text{Mo}_{10}\text{Al}_5$ in the composition space

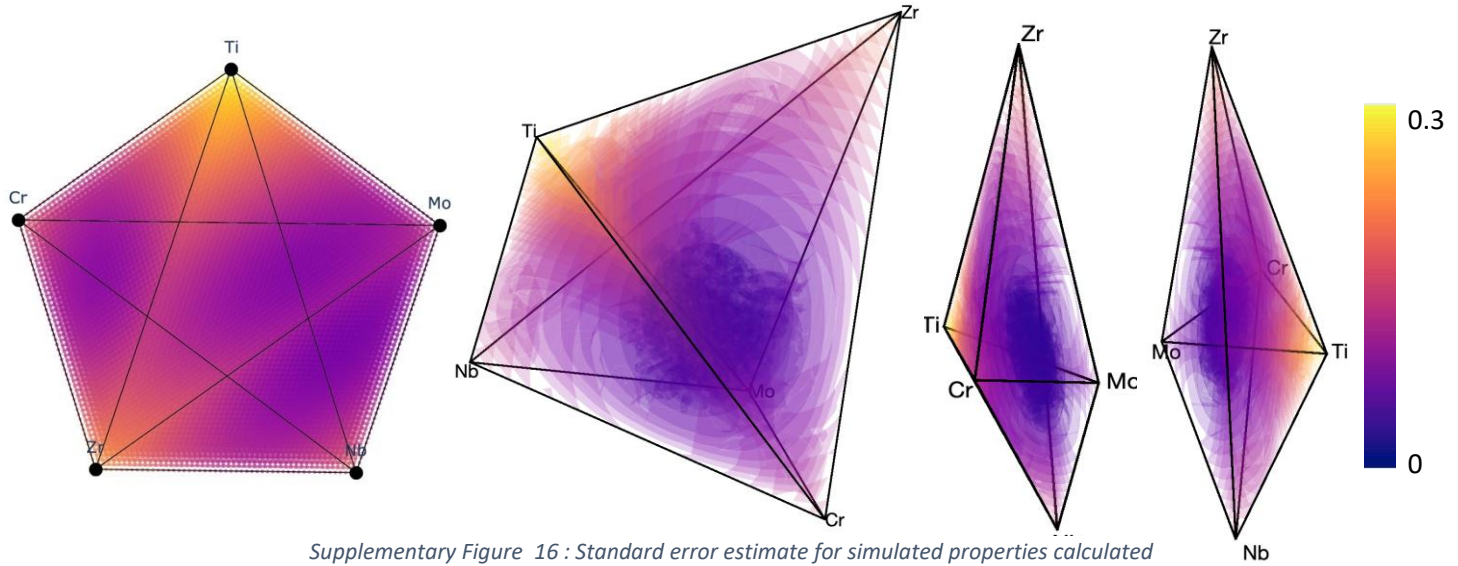
Supplementary Note 5: Model error distribution

The prediction error can be computed as:

$$\frac{s_{\hat{y}_i}}{s} = \sqrt{x_i^T (X^T X)^{-1} x_i}$$

Where s is the expected prediction error, $s_{\hat{y}_i}$ the prediction error, x_i the i^{th} points coordinate, X the experimental points matrix and thus $X^T X$ variance-covariance matrix (supplementary Figure 16)¹¹.

The value of standard error estimates in each point is computed and plotted.



Supplementary Figure 16 : Standard error estimate for simulated properties calculated from our experimental dataset compositions.

Without surprise, the model error is maximal where the experimental data are scarce, typically close to the Ti and Zr vertices and along binaries in general (those were not included into this study).

Precisions of Young Modulus of the different components compared to theoretical values give :

Cr	267 GPa predicted	vs	279 GPa theoretically	(3% error)
Mo	330 GPa predicted	vs	330 GPa theoretically	(0% error)
Zr	126 GPa predicted	vs	88 GPa theoretically	(40% error)
Ti	133 GPa predicted	vs	108 GPa theoretically	(23% error)
Nb	207 GPa predicted	vs	105 GPa theoretically	(97% error)

As expected, Mo and Cr elastic modulus are well predicted, while for Ti and Zr the error is near 30%. For Nb, the huge error may not come from the coverage of the zone but more on the difficulty to deconvolute the influence of each pure element on the properties, as the dataset does not contain the pure compositions but only mixtures. While approaching Nb, the Young modulus prediction is indeed very unstable and oscillate between 207 GPa and 140 GPa. The vertices correspond to limit cases for

the model, causing possible instability. Adding pure elements mechanical properties is thus necessary if focusing on the border of the domain.

Supplementary Note 6: Machine Learning models

1. Data gathering and treatments: the different datasets

Datasets are available in the repository [Accelerated exploration of multinary systems | Zenodo](#)

Raw data:

It contains all compositions, EBSD IQ and CI, 5 replications of E and H measured by -oindentation and corrected with Oliver and Pharr models.

In the repository, “Raw_data.csv” contains the data without any correction on E and H, and “Raw_data_corrected.csv” dataset contains the Oliver Pharr “corrected” data, using fused silica calibration.

Threshold data:

Some nano-indentation test failures and sample inhomogeneities lead to values of elastic modulus and hardness that are physically inconsistent. All compositions with an H value under 2 GPa and an E value under 10 GPa are removed from the dataset.

In the repository, this corresponds to “Raw_data_corrected_threshold.csv”.

Statistically processed data:

nano-indentation data are statistically processed, considering the indents corresponding to a same composition as a statistical sample. For each thresholded quantity E and H, outliers are extracted from these replications using Dixon Q-test⁵¹ on the minimum and on the maximum (independently).

In the repository, the statistical treatment on elastic modulus gives “Composition_E_wo_outliers” and the treatment applied on H produces “Composition_H_wo_outliers”.

Averaged statistically processed data:

An averaged database is computed by associating each composition to corresponding IQ and CI, and to the mean value and standard deviation of E and H replications (with removed outliers). CI is used to define EBSD classes that are added to the dataset: compositions with a CI<0.02 are classified as amorphous, while those with CI>0.02 are classified as crystalline.

In the repository, this dataset is given as “Database_averaged_without_outliers”.

XRD classes:

XRD patterns are only analyzed as “crystalline” or “amorphous” depending on the presence or absence of peaks, corresponding to 0 and 1 level, which are used for classification models.

XRD classes associated with the composition constitute another dataset “Database_XRD.csv”

Properties associated to compositions with 2%at variations are predicted from the previous datasets and Machine Learning models. From the mechanical properties of the Statistically processed data, i.e. elastic modulus and hardness, Galanov’s model⁵ allows to compute the relative characteristic size of the elastic-plastic zone under the indenter $\frac{b_s}{c}$, the constraint factor C (H=C. σ with σ the flow stress)

and ductility characteristic δ_H from E and H predictions using a numerical resolution of the system proposed by Galanov.

In the repository, the databases “Predictions_NN_mechanical_model”, “Predictions_RF_mechanical_model”, and “Predictions_SVM_mechanical_model” contains these modeled data.

2. Regression scores

Expected and predicted data on a test set are ideally equals, meaning that a regression between these data should have an adjusted coefficient of determination R^2_{adj} close to 1 (considering there is no lack of fit). Absolute Error (MAE) also gives the distance between expected and predicted value, which is physically more meaningful.

3. Classification score

Accuracy score is the number of true predictions among all predictions. Weighted average F1-score (called F1-score in the paper) is the weighted average of ratios between True Positive, False Positive and False Negative for both class⁵²: this score takes into account the whole confusion matrix and is considered as a good indicator. Hamming loss is the fraction of wrong predictions among all predictions, it should be (1-accuracy) for two classes.

4. Models assessment

Model assessment is performed for Multiple Regression (MR), Support Vector Machine (SVM), Random Forest (RF) and Neural Network (NN) models using iterative cross-validation method, with 5 folds and 30 iterations.

Iterative k-fold cross-validation consists in dividing datasets into k folds that are successively used as train data or test data. Here $k=5$, meaning that the models are successively trained with 4 folds and tested with the fifth. Iterative cross-validation allows repeating n times this k-fold cross-validation. Here $n=30$, so the data are shuffled and sliced into k-fold 30 times. At the end, the model is trained and tested (or evaluated) $30 \times 5 = 150$ times. This allows having a significant mean value and standard deviation for the evaluation metrics. A wide distribution of the metrics shows that model performance is sensitive to the choice of train dataset for instance, while the mean value of the distribution is an indicator of the quality of the model that fits or classes the data.

To minimize the effect of the experimental errors as much as possible, the datasets used to assess the best model architectures are the ones that were, if applicable, thresholded and processed by a Dixon Q-test, meaning the ones with the lowest amount of outliers (“statistically processed data”)

- Elastic modulus is fitted from Compo_E_wo_outliers dataset
- Hardness is fitted from Compo_H_wo_outliers dataset
- CI and IQ are fitted Data_averaged dataset
- Phase classification from EBSD data is performed from Data_averaged dataset
- Phase classification from XRD data is performed from Database_XRD dataset

Selection of the best hyperparameters is based on the best regression adjusted coefficient of determination R^2_{adj} between expected and predicted values of a test set or, for classification, by weighted averaged F1-score. The relevance of these metrics was validated by studying correlation diagrams for R^2_{adj} , and confusion matrix, accuracy and Hamming loss metrics for F1-score. Results are given in Supplementary Tables 10 to 16.

The use of one set of hyperparameters for each type of model, selected with one particular dataset, introduces a bias when comparing model performances in different datasets. We nevertheless made this choice in order to be able to compare the effect of removing outliers.

Trained models and training data are available in this repository : [Accelerated exploration of multinary systems | Zenodo](#)

Code to perform such trainings are available in GitLab: <https://gricad-gitlab.univ-grenoble-alpes.fr/garele/accelerated-exploration-of-multinary.git>

A Ph.D. thesis covering more details on this study and complementary analysis is also available for reading <https://cnrs.hal.science/tel-04043261v1>

5. Best models hyperparameters

- Multilinear regression (MR):

Quartic models (with Scheffé interactions⁵³) was selected using the statsmodels library in Python for the regression of Young's Modulus, Hardness and EBSD CI and IQ.

$$\begin{aligned} y = & \sum_{1 \leq i \leq q} \beta_i x_i + \sum_{1 \leq i \leq j \leq q} \beta_{ij} x_i x_j + \sum_{1 \leq i \leq j \leq q} \gamma_{ij} x_i x_j (x_i - x_j) + \sum_{1 \leq i \leq j \leq k \leq l \leq q} \beta_{ijkl} x_i x_j x_k x_l \\ & + \sum_{1 \leq i \leq j \leq k \leq q} \beta_{ijk} x_i^2 x_j x_k + \sum_{1 \leq i \leq j \leq k \leq q} \beta_{ijk} x_i x_j^2 x_k + \sum_{1 \leq i \leq j \leq k \leq q} \beta_{ijk} x_i x_j x_k^2 \\ & + \sum_{1 \leq i \leq j \leq q} \delta_{ij} x_i x_j (x_i - x_j)^2 \end{aligned}$$

- Support Vector Model (SVM):

Regression and classification were performed using Scikit-learn SVM library of Python, in our PyTerK environment. The hyperparameters are the kernel function, the proportion of support vectors ν and the penalty parameter C. Young's modulus and hardness are modelled with nuSVR Scikit-learn class, with an RBF (Radial Basis Function) kernel, ν equal to 0.5 and C equal to 1000. Regression over CI is performed with a nuSVR class, RBF kernel, ν equal to 0.8 and C equal to 100. Regression over IQ is performed with an SVR class, degree 3 polynomial kernel, ν equal to 0.2 and C equal to 1000. Phase classification from EBSD and XRD classes is done with an SVC class, RBF kernel and C equal to 100.

- Random Forest (RF):

Regression and Classification is performed using Scikit-learn Random Forest library of Python, in our PyTerK environment. The hyperparameters are the number of estimators and the minimum number of samples per leaf that allows the split. Regressions are done with RandomForestRegressor Scikit-learn class, classifications with RandomForestClassifier class. The elastic modulus is modelled with 100 estimators and 10 minimum samples for splitting. Hardness is modelled with 150 estimators and 10 minimum samples for splitting. CI is modelled with 150 estimators and 5 minimum samples for splitting. IQ is modelled with 50 estimators and 5 minimum samples for splitting. Phase classifications from EBSD and XRD are performed with 150 estimators and 5 minimum samples for splitting.

- Neural Network (NN):

Regression and Classification is performed using Tensorflow/Keras library of Python, in our PyTerK environment. The optimizer is the Adam stochastic gradient descent method. The hyperparameters are

the number of layers and the number of neurons per layer. All activation functions are ReLU (Rectified Linear Unit), and a sigmoid layer is added for classification. All models are Keras Sequential models. Elastic modulus, Hardness and IQ are best predicted with 100x100x100x100 hidden layers. CI is modelled by 50x100x100x50 hidden layers. Phase classifications from EBSD and XRD are performed by 50x50x100x100 hidden layers.

6. Regression over mechanical properties

Optimized models are trained for Young's Modulus (E) and Hardness (H) predictions over the different datasets, gathering raw experimental results to statistically processed data where outliers on replications of nano-indentation measurements were removed.

Model quality is quantified through computation of the adjusted coefficient of determination R^2_{adj} of the regression between expected and predicted values of a test set, using iterative k-fold cross validation. These regressions present no visible lack of fit, which makes the R^2_{adj} an accurate metric (see Supplementary Figure 29 to Supplementary Figure 36). R^2_{adj} mean values and standard deviation over 30×5 successive trainings are given in Supplementary Table 3 and Supplementary Table 4.

It appears clearly that the removal of outliers on -oidents replications is systematically associated with a significant increase the R^2_{adj} mean value, and with the decrease of the R^2_{adj} standard deviation, for both outputs. For instance, with hardness output, RF model associated R^2_{adj} goes from 0.751 ± 0.052 with raw data (mean $R^2_{adj} \pm$ standard deviation), to 0.963 ± 0.009 with processed data. This implies that performance of the models increases, unsurprisingly, with the quality of the dataset.

Averaging E and H replications for the same composition — from “Statistically processed data” to “Averaged statistically processed data”—, lead to a reduction of the dataset size that can be disadvantageous to some families of models. It appears that RF is more sensitive to a decreasing size of dataset than MR, SVM or NN.

RF and NN models trained with “Statistically processed data” give the best predictions, with similar performances, for elastic modulus and hardness. The adjusted coefficient of determination is close to 0.970 for E and 0.963 for H, with a standard deviation closed to 0.01. Meanwhile, the Mean Absolute Error (MAE) distribution (see Supplementary Figure 31 and Supplementary Figure 35) shows an average close to 6.5 GPa for E and to 0.35 GPa for H. In comparison, the mean standard deviations on experimental assessment of E and H (with removed outliers) are 5.94 GPa and 0.34 GPa, respectively. This means that modeling E and H with an RF or an NN model introduces a bias similar to the intrinsic experimental error.

Although MR is clearly not the best predictive model — R^2_{adj} being 0.951 ± 0.010 for E modelling and 0.916 ± 0.013 for H modelling from “Statistically processed data” — it is sufficient to have a reliable prediction of the Young's modulus and a good approximation of hardness. It allows having a direct insight of the effect of interactions between elements on the mechanical properties. The quartic multiple regression coefficients (SeeSupplementary Figure 27 and Supplementary Figure 28) reveal that the elastic modulus depends almost linearly on Zr, Nb, Cr and Mo, while Ti has no significant influence on it. The effect of the interactions between these components on the elastic modulus are very low. On the contrary, binary interactions have a strong positive effect on hardness, while three and four component interactions have no effect or a negative effect on hardness. This is not in favor of the cocktail effect, often given as a leading property of HEA and metallic glasses, and suggests that its systematic association with multinary alloys should be taken with caution.

Supplementary Table 3: Regression adjusted coefficient of determination R^2_{adj} of test vs predicted values of Young Modulus

Regression models	Mean adjusted $R^2 \pm$ adjusted R^2 standard deviation for datasets:			
	Raw data	Threshold data	Statistically processed data	Averaged statistically processed data
MR	0.811 ± 0.040	0.910 ± 0.028	0.951 ± 0.010	0.953 ± 0.017
RF	0.810 ± 0.040	0.923 ± 0.027	0.970 ± 0.012	0.938 ± 0.020
SVM	0.822 ± 0.044	0.917 ± 0.028	0.957 ± 0.010	0.960 ± 0.010
NN	0.822 ± 0.040	0.926 ± 0.031	0.967 ± 0.011	0.968 ± 0.009

Supplementary Table 4: Regression adjusted coefficient of determination R^2_{adj} of test vs predicted values of Hardness

Regression models	Mean adjusted $R^2 \pm$ adjusted R^2 standard deviation for datasets:			
	Raw data	Threshold data	Statistically processed data	Averaged statistically processed data
MR	0.710 ± 0.046	0.847 ± 0.037	0.916 ± 0.013	0.906 ± 0.030
RF	0.751 ± 0.052	0.889 ± 0.035	0.963 ± 0.009	0.921 ± 0.021
SVM	0.743 ± 0.058	0.879 ± 0.037	0.946 ± 0.012	0.938 ± 0.024
NN	0.750 ± 0.051	0.889 ± 0.039	0.964 ± 0.008	0.966 ± 0.011

7. Regression and classification over phase transition

Phase prediction is performed by training each regression ML model with datasets associating compositions to EBSD CI and IQ, and each classification model with compositions associated to EBSD and XRD phase classes (see Supplementary Figure 37 to Supplementary Figure 40 and Supplementary Table 5 to Supplementary Table 8). Regression over EBSD indicators is not really convincing, with an averaged R^2_{adj} of 0.9 at best, with RF model: the dataset is quite small as there is only one CI and IQ measurement per composition. IQ values predicted by SVM and NN are especially off, which is why the CI was kept and thresholded to define phase classes. Classification performances are evaluated by the F1 score, accuracy, Hamming loss and confusion matrices (see Methods). The best phase class prediction is performed with a Neural Network model giving F1 score and accuracy close to 0.95 for both EBSD and XRD phase class.

Supplementary Table 5: Regression adjusted coefficient of determination R^2_{adj} of test vs predicted values of EBSD Confidence Index (CI)

Regression models	Mean adjusted $R^2 \pm$ adjusted R^2 standard deviation for dataset:
	Averaged statistically processed data
MR	0.840 ± 0.069
RF	0.899 ± 0.057
SVM	0.936 ± 0.040
NN	0.945 ± 0.040

Supplementary Table 6: Regression adjusted coefficient of determination R^2_{adj} of test vs predicted values of EBSD Image Quality (IQ)

Regression models	Mean adjusted $R^2 \pm$ adjusted R^2 standard deviation for dataset:
	Averaged statistically processed data
MR	0.869 ± 0.053
RF	0.902 ± 0.056
SVM	0.642 ± 0.100
NN	0.745 ± 0.062

Supplementary Table 7: Evaluation of EBSD phase classification

Classification models	Evaluation of classification on dataset Averaged statistically processed data		
	F1-score	Accuracy	Hamming loss
RF	0.942 ± 0.023	0.942 ± 0.023	0.058 ± 0.023
SVM	0.942 ± 0.021	0.942 ± 0.021	0.058 ± 0.021
NN	0.958 ± 0.024	0.958 ± 0.023	0.042 ± 0.023

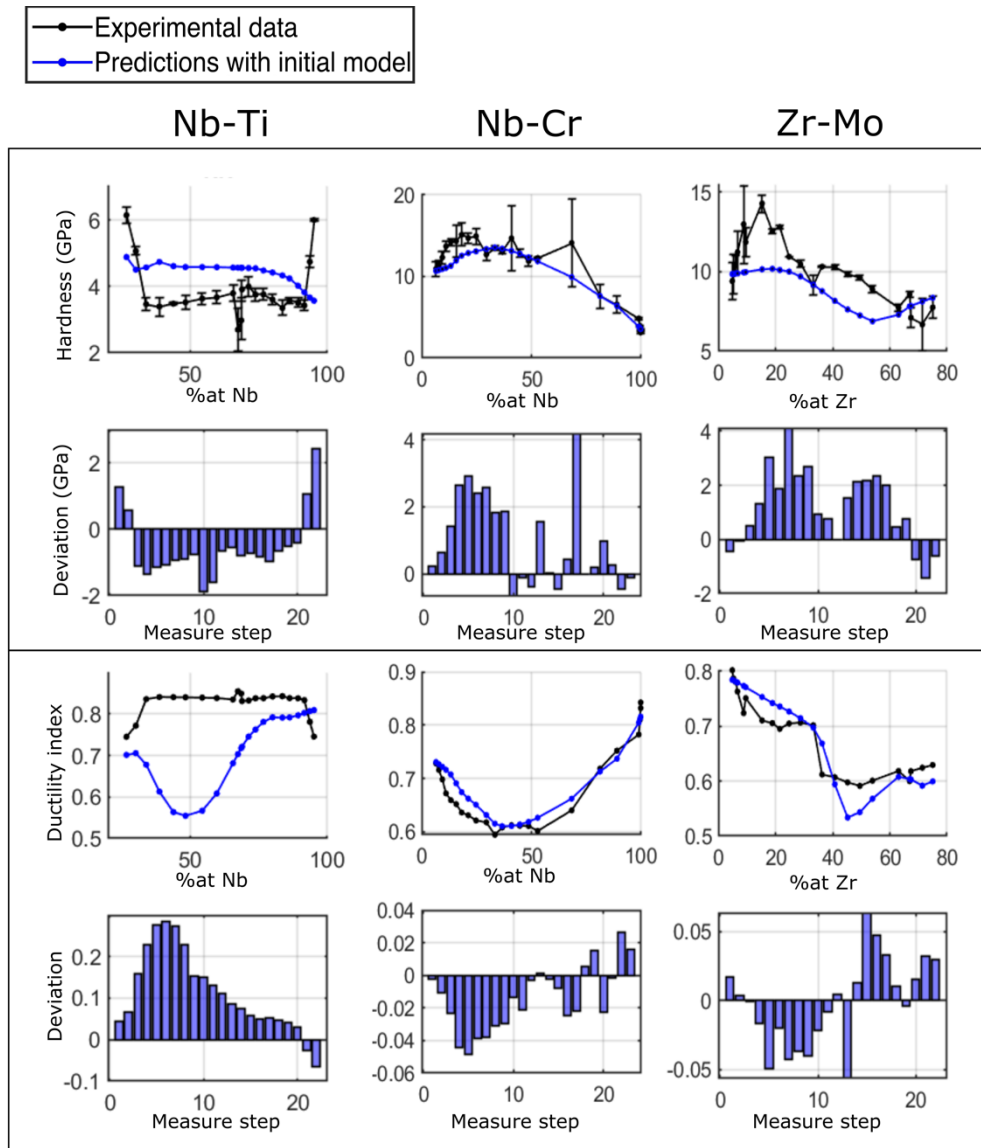
Supplementary Table 8: Evaluation of XRD phase classification

Classification models	Evaluation of classification on dataset XRD classes		
	F1-score	Accuracy	Hamming loss
RF	0.926 ± 0.028	0.926 ± 0.029	0.074 ± 0.028
SVM	0.939 ± 0.023	0.939 ± 0.023	0.061 ± 0.023
NN	0.947 ± 0.027	0.947 ± 0.026	0.053 ± 0.026

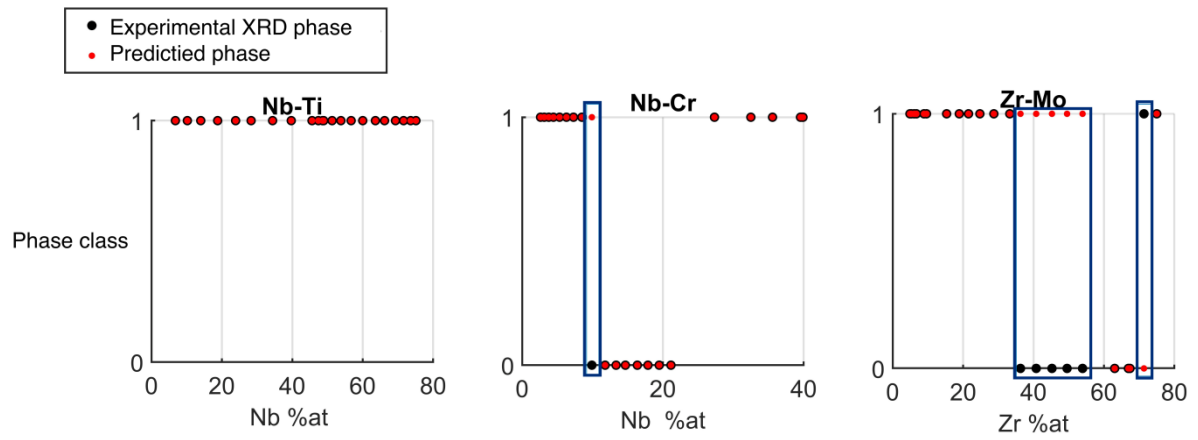
Supplementary Note 7: Binaries validation set

Three binary samples were fabricated as validation set. We chose Nb-Ti which is a vertex far from initial experimental dataset points, and which is supposed to be entirely crystallized according to prediction. Nb-Cr and Zr-Mo on the contrary show a phase class variation along the gradients. Nb-Cr is closer to experimental points which allow to compare the model predictivity depending the model error value.

Comparison between experimental values and predicted values are shown in Supplementary Figure 17: as expected, the prediction error is lower on Nb-Cr. Supplementary Figure 18 shows that phase classes are correctly predicted on Nb-Ti and a phase class variation along the gradient is also correctly predicted on Nb-Cr and Zr-Mo, although the exact position of the phase change is not correctly predicted, particularly on Zr-Mo.

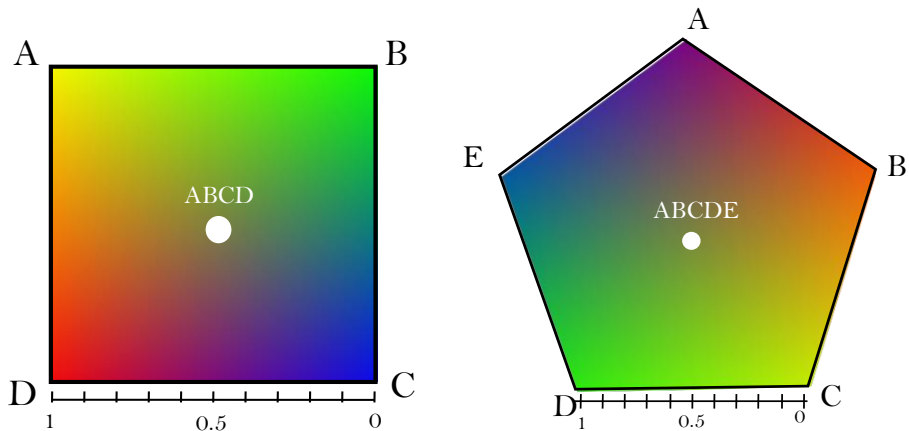


Supplementary Figure 17: Prediction-experience deviation along the binary gradients

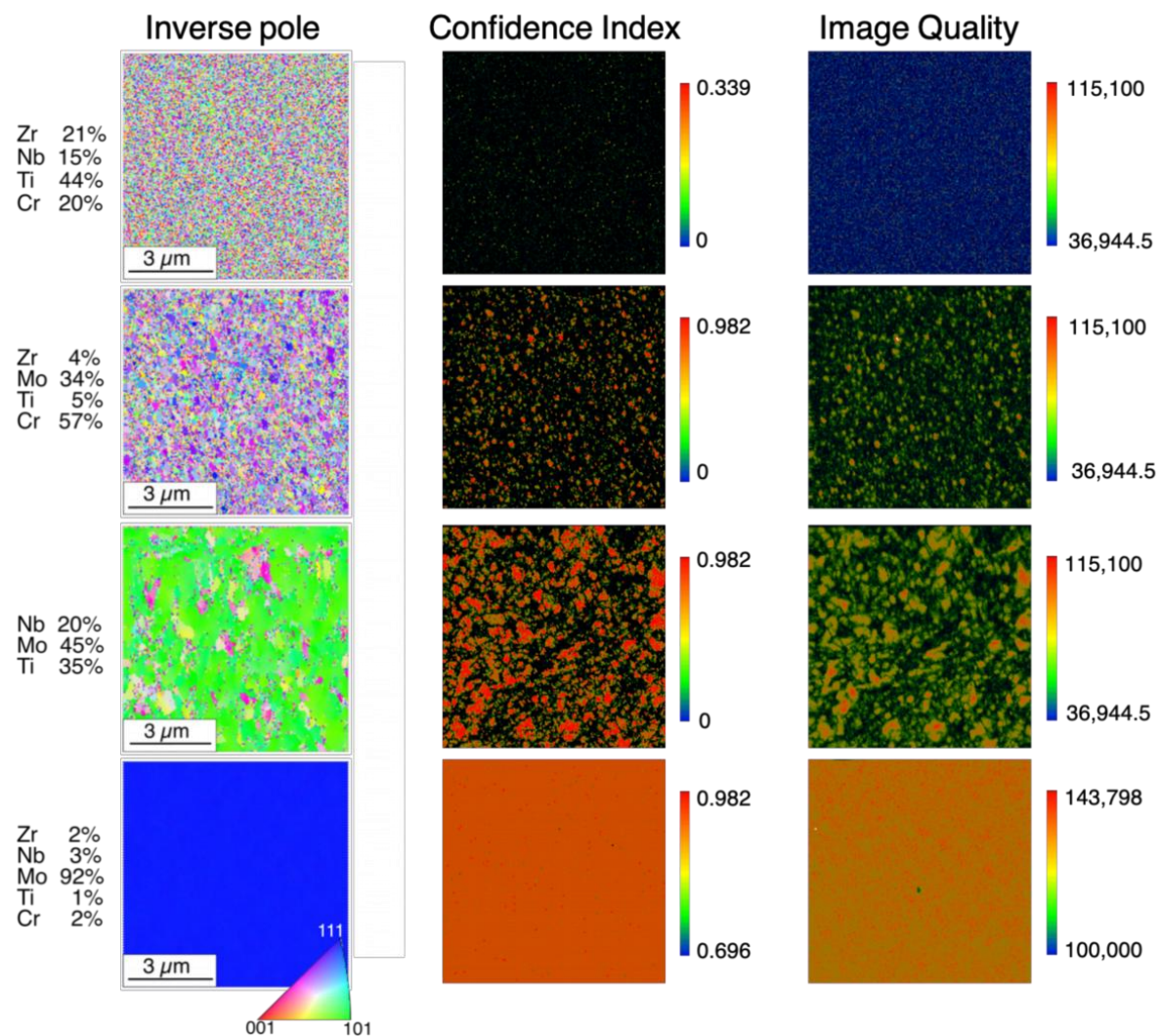


Supplementary Figure 18: Predicted phase class vs experimental XRD phase class for the three binaries

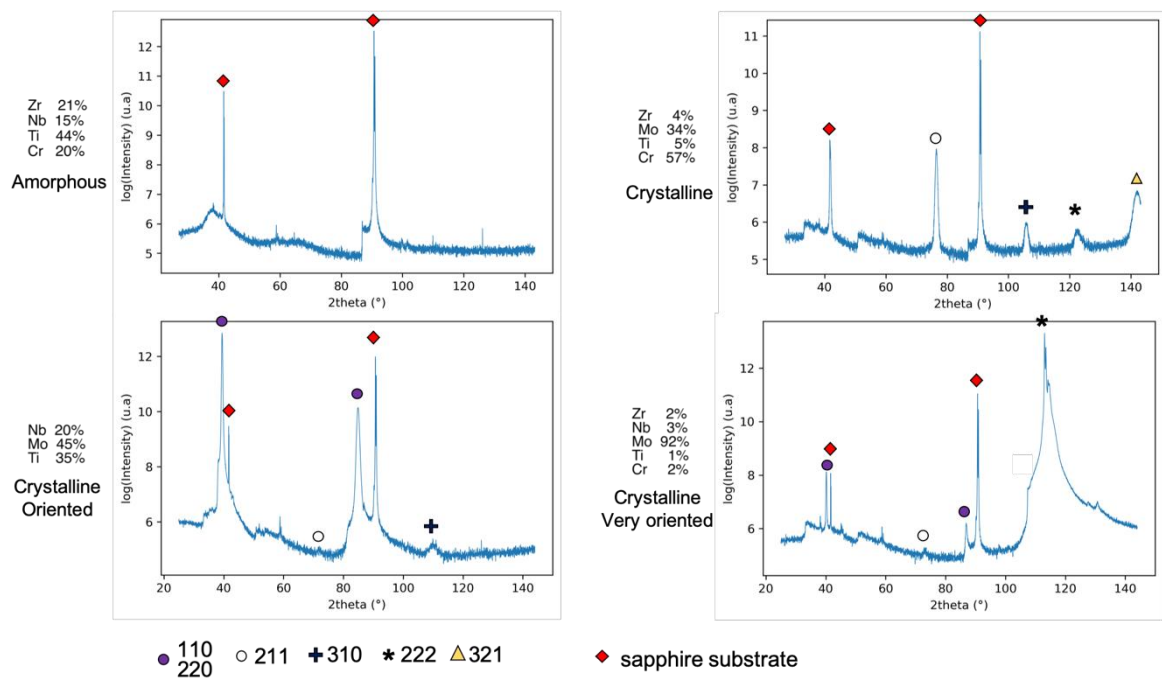
Supplementary Figures



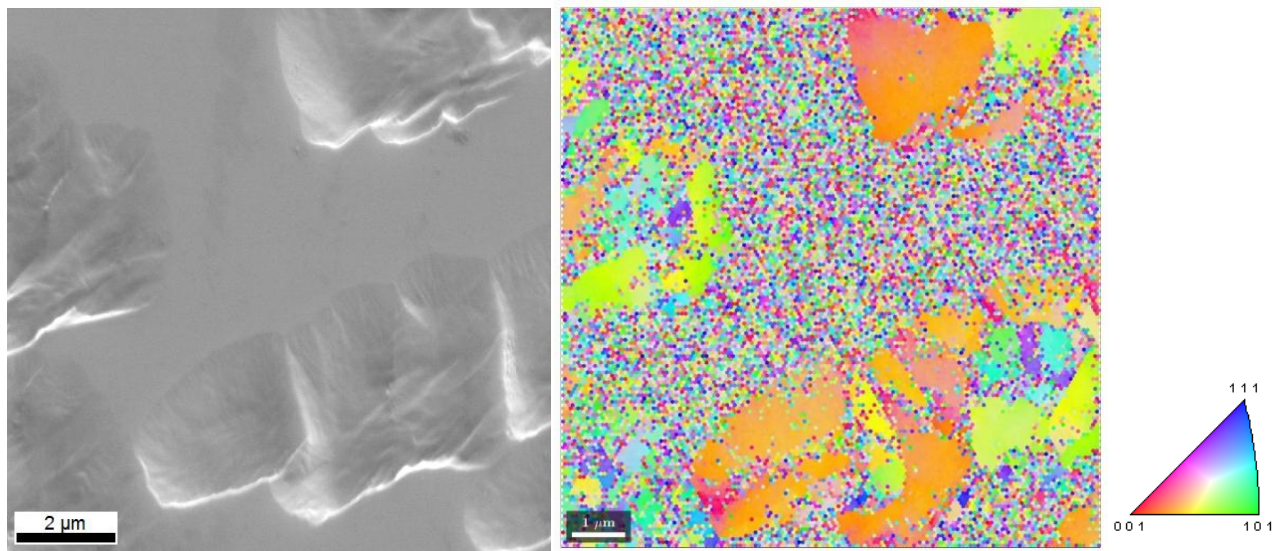
Supplementary Figure 19: Sample map of a quaternary A-B-C-D screened with four cathodes and of a quinary A-B-C-D-E screened with five cathodes. The map corresponds to a projection of the 3D and 4D composition spaces in 2D leading to an overlapping of some mixtures. In the quaternary, AC and BD mixtures cannot be obtained; in both mixtures, ternary cannot be obtained either. Using more than three cathodes is then inefficient to guarantee a regular screening of the composition space on a 2D substrate.



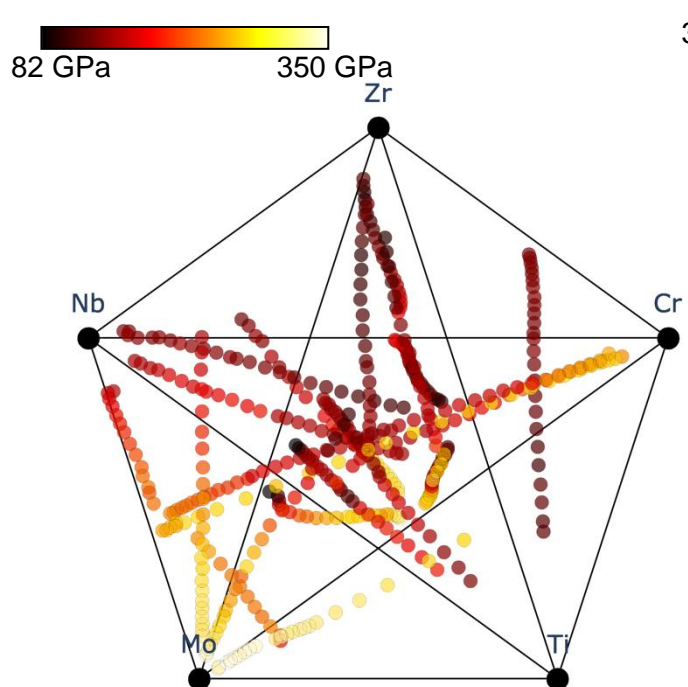
Supplementary Figure 20 : EBSD maps for 4 compositions, as Inverse Pole figure, Confidence Index map and Image Quality map, from amorphous to almost single crystal.



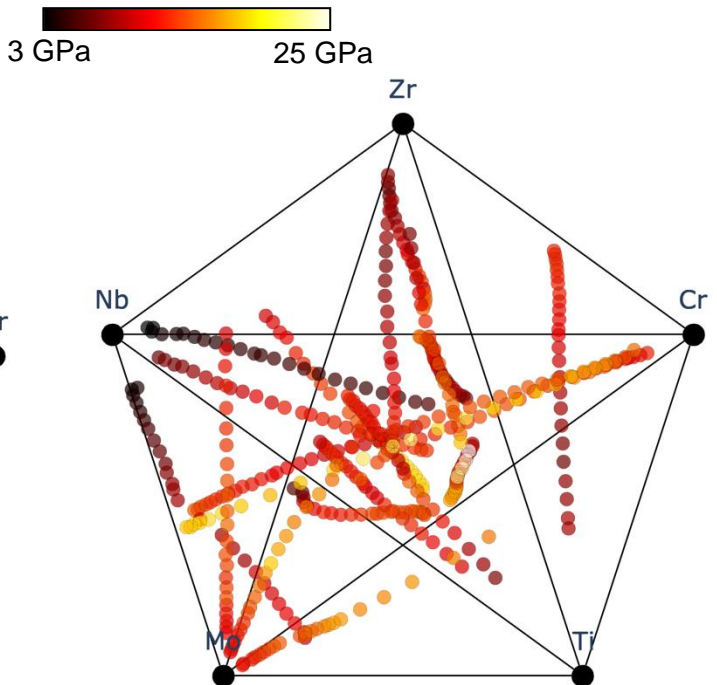
Supplementary Figure 21: XRD diffraction patterns for 4 compositions, from amorphous to almost single crystal.



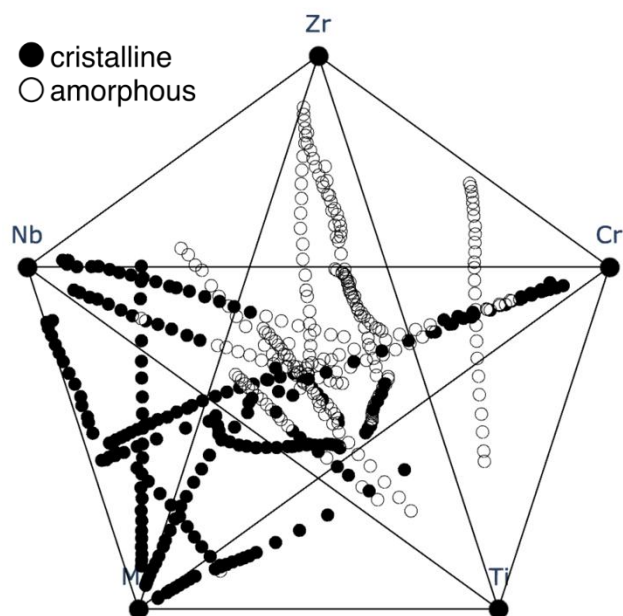
Supplementary Figure 22: SEM image of $Zr_9Nb_{40}Mo_{17}Ti_{13}Cr_{21}$ and corresponding EBSD map. Due to substrate bias, ion bombarding has locally etched the surface. The surface appears amorphous on the EBSD map, with very badly defined orientations. The crystalline zones are on the contrary corresponding to etched zones. XRD shows diffraction peaks for this composition.



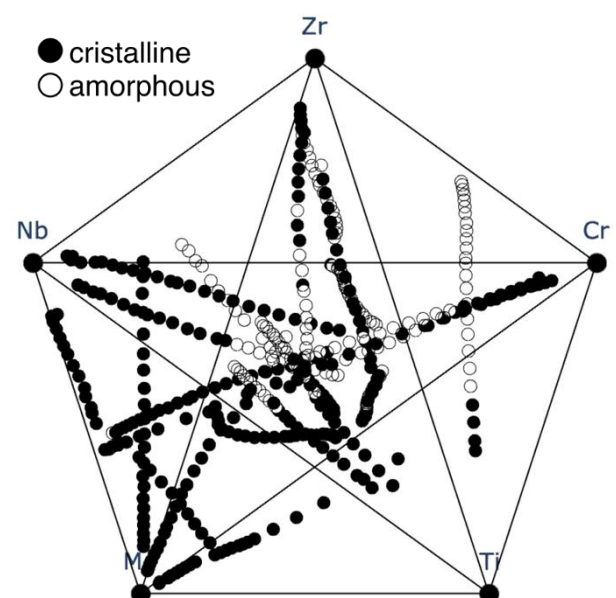
Supplementary Figure 23: Experimental value of elastic modulus



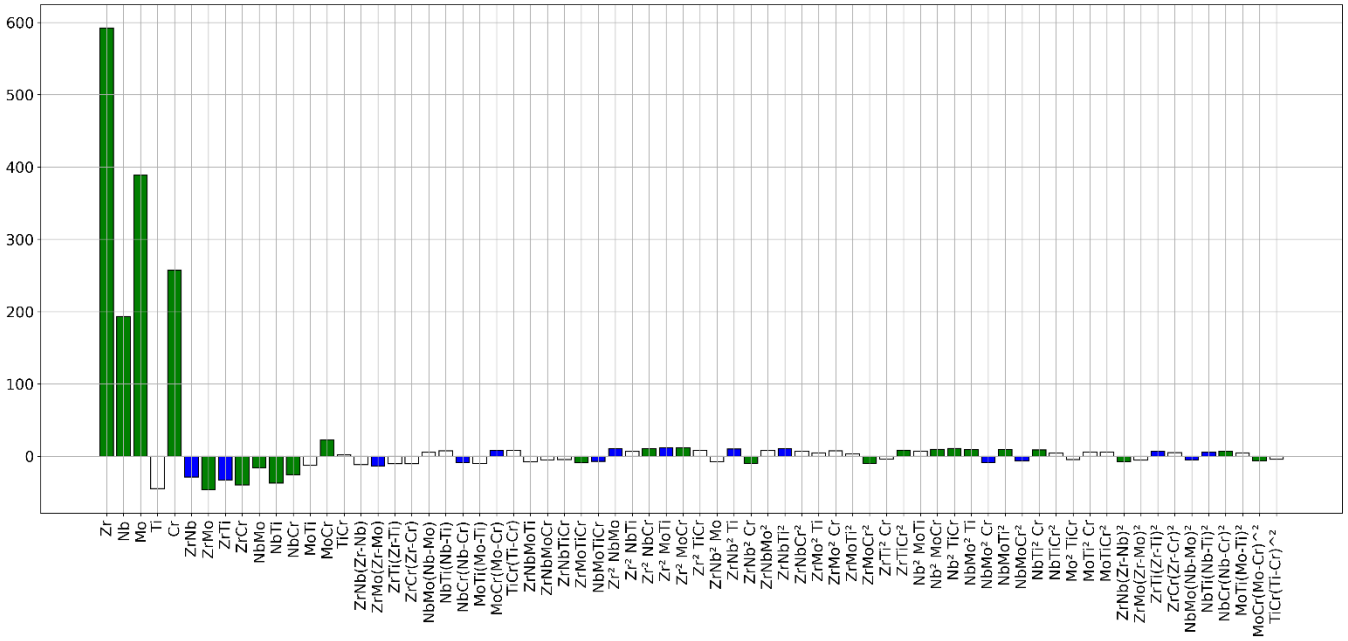
Supplementary Figure 24: Experimental value of hardness



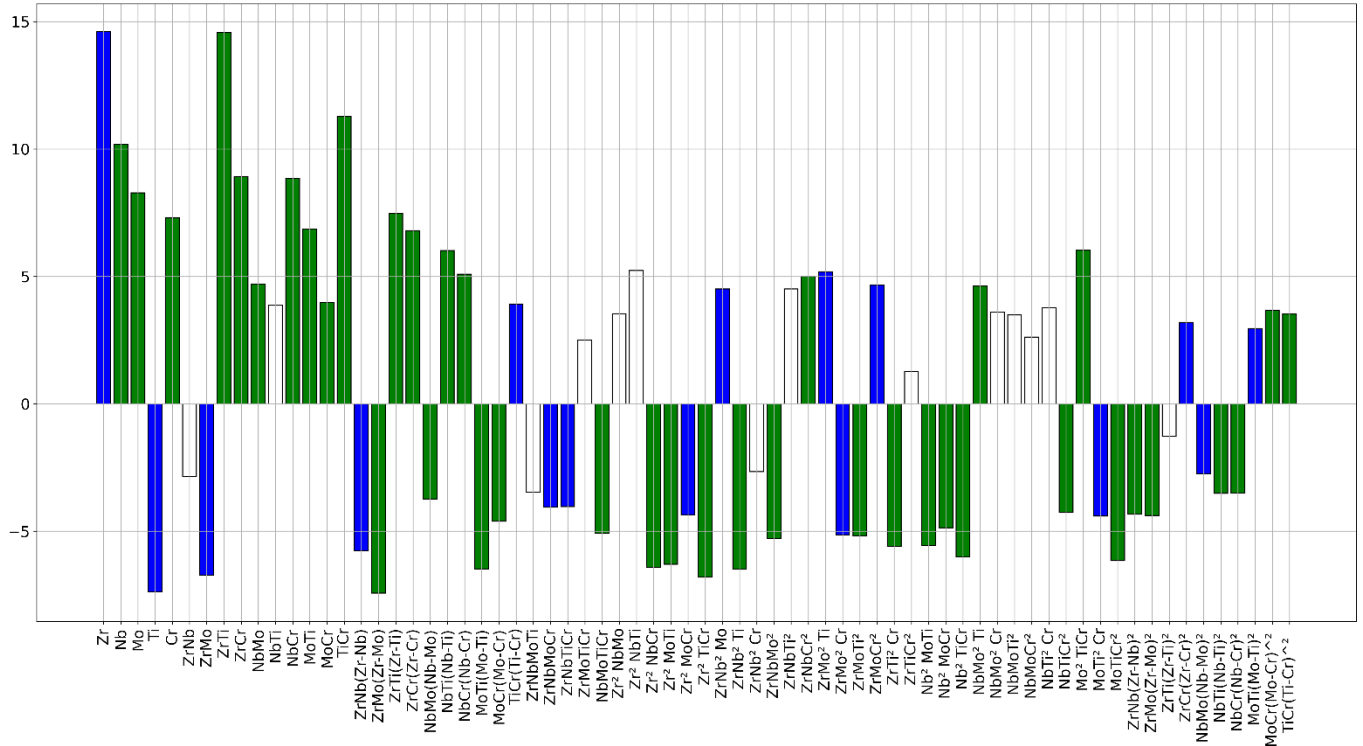
Supplementary Figure 25 : EBSD experimental phase class



Supplementary Figure 26: XRD experimental phase class

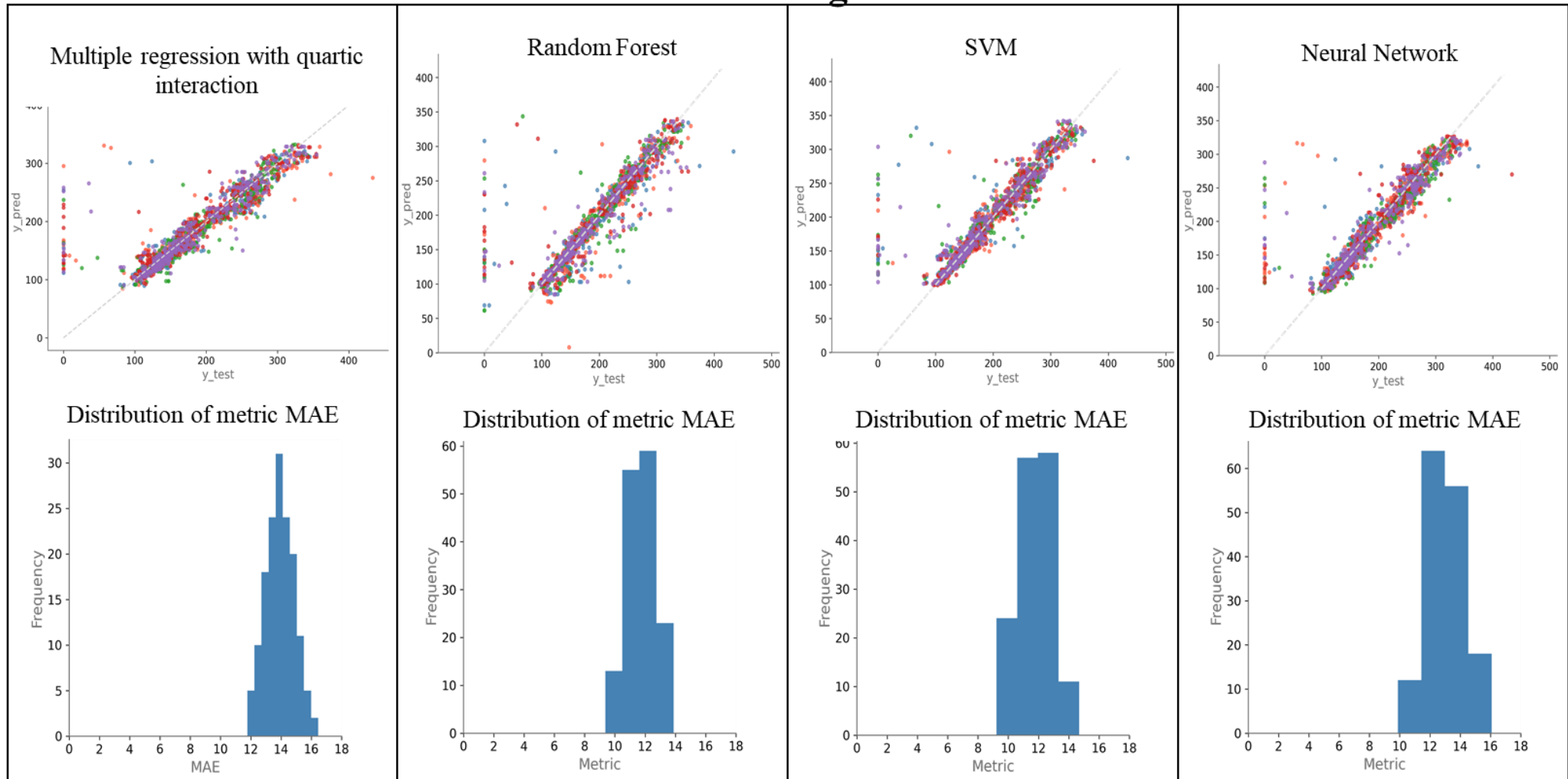


Supplementary Figure 27 : Coefficients of quartic multiple regression on Young Modulus. Coefficient C_i corresponding to an interaction terms of degree n are plotted as $(C_i)^{1/n}$. Bar color depends on the p -value of the hypothesis H_0 that the coefficients C_i are equal to zero, meaning that the associated parameter or interaction has no influence on the response. Coefficients with p -value = 0 (significant) are plotted in green, $0 < p$ -value < 0.05 are plotted in blue, p -value > 0.05 (non-significant) are plotted in white.



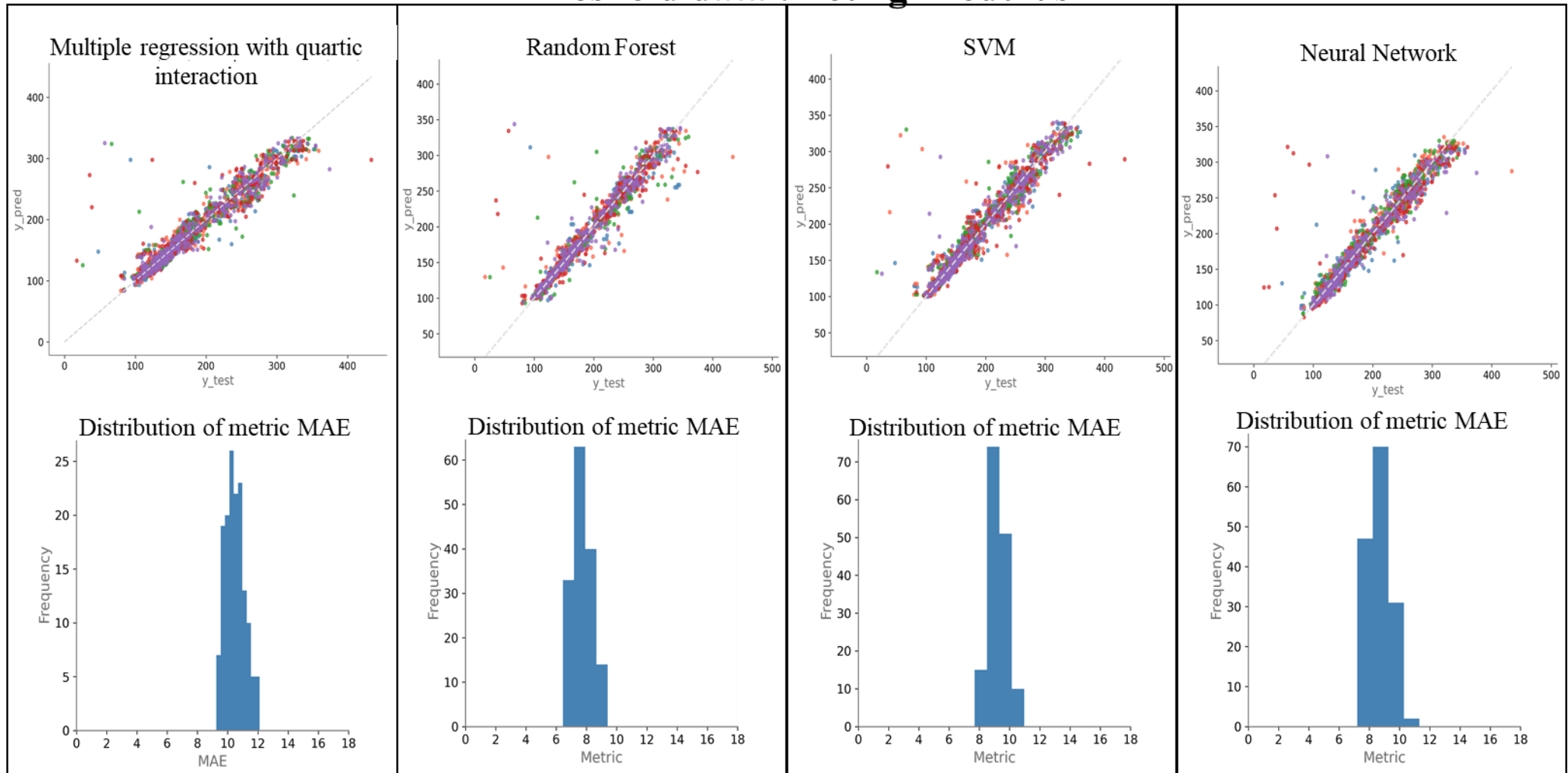
Supplementary Figure 28: Coefficients of quartic multiple regression on Hardness. Coefficient C_i corresponding to an interaction terms of degree n are plotted as $(C_i)^{1/n}$. Bar color depend on the p -value of the hypothesis H_0 that the coefficients C_i are equal to zero, meaning that the associated parameter or interaction has no influence on the response. Coefficients with p -value = 0 (significant) are plotted in green, $0 < p$ -value < 0.05 are plotted in blue, p -value > 0.05 (non-significant) are plotted in white

Raw data : Young Modulus



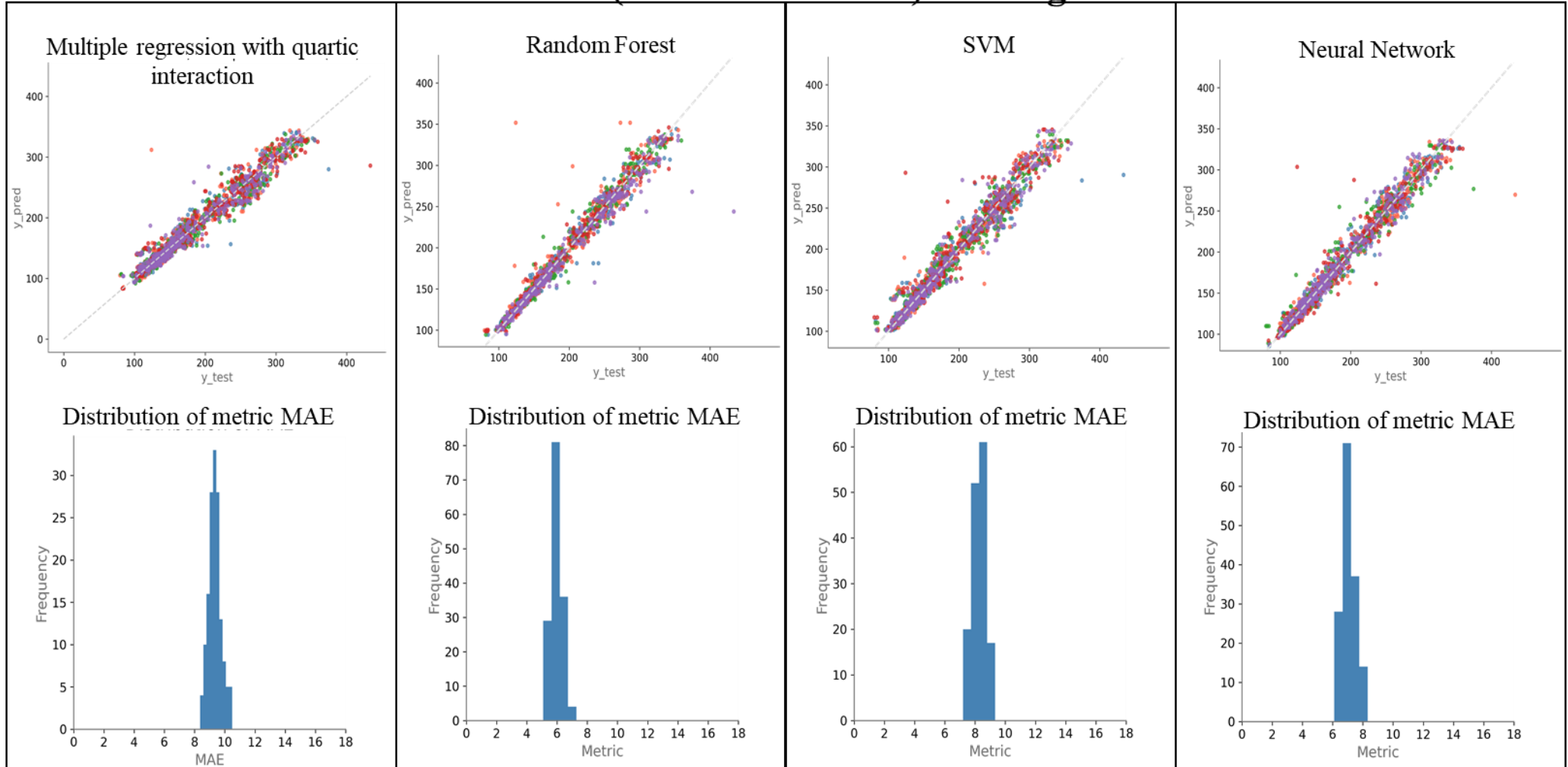
Supplementary Figure 29: Regressions between predicted and expected values on test sets of elastic modulus, and MAE metric distribution for different Machine Learning models, with "Raw data" datasets

Threshold data : Young Modulus



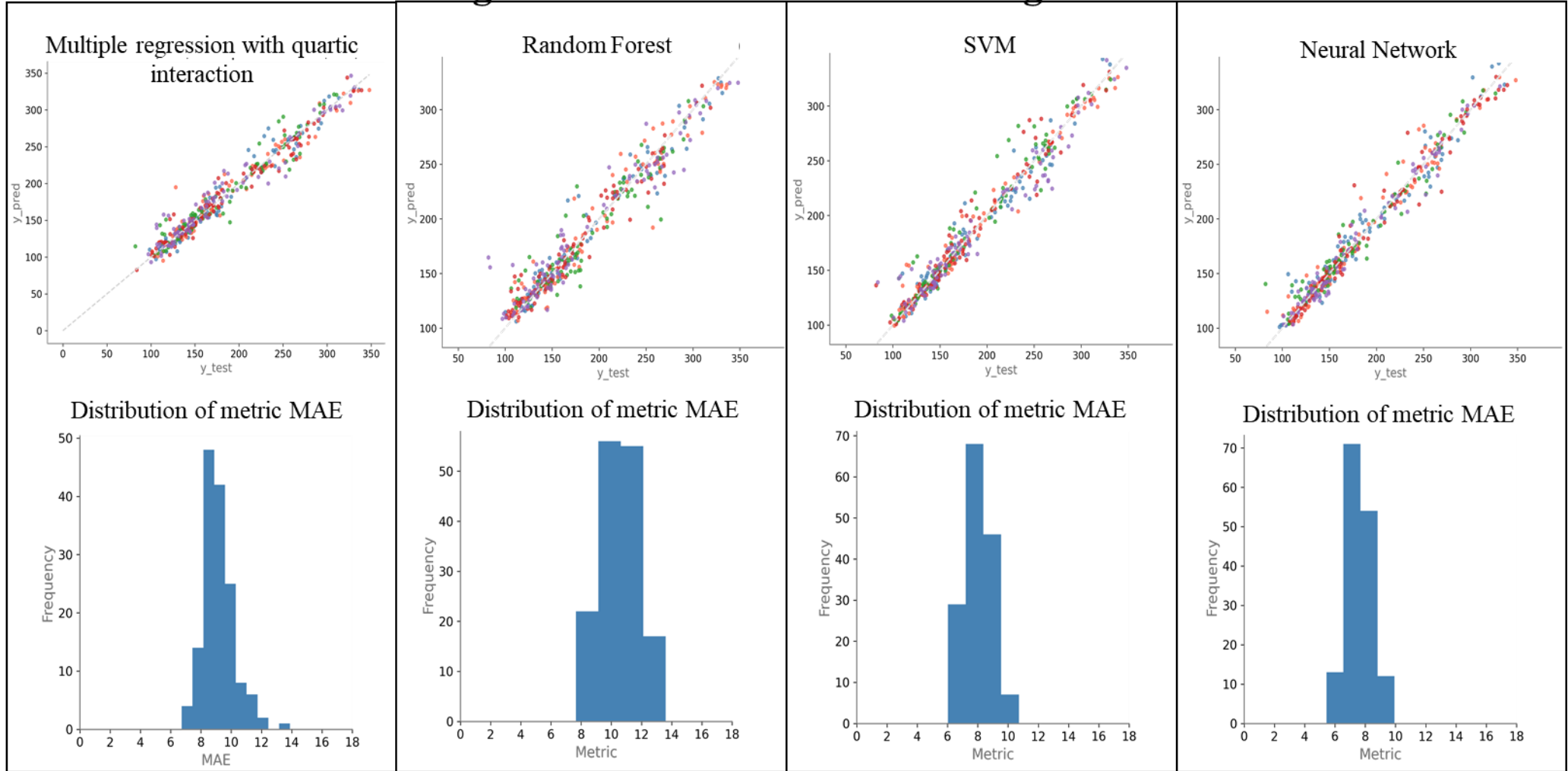
Supplementary Figure 30: Regressions between predicted and expected values on test sets of elastic modulus, and MAE metric distribution for different Machine Learning models, with "Threshold data" dataset

Processed data (outliers removed) : Young Modulus



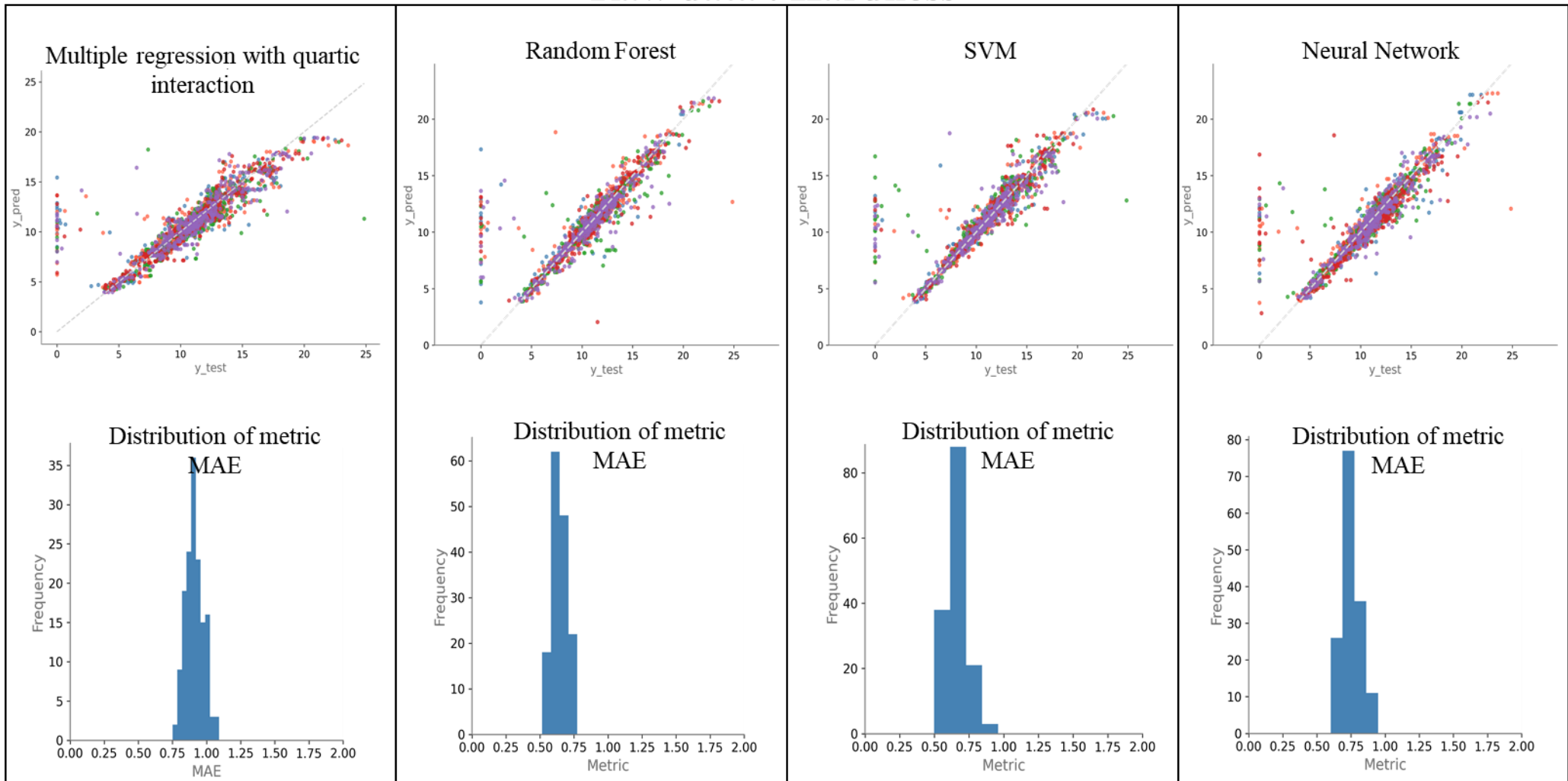
Supplementary Figure 31: Regressions between predicted and expected values on test sets of elastic modulus, and MAE metric distribution for different Machine Learning models, with "Statistically processed data" dataset

Averaged data without outliers : Young Modulus



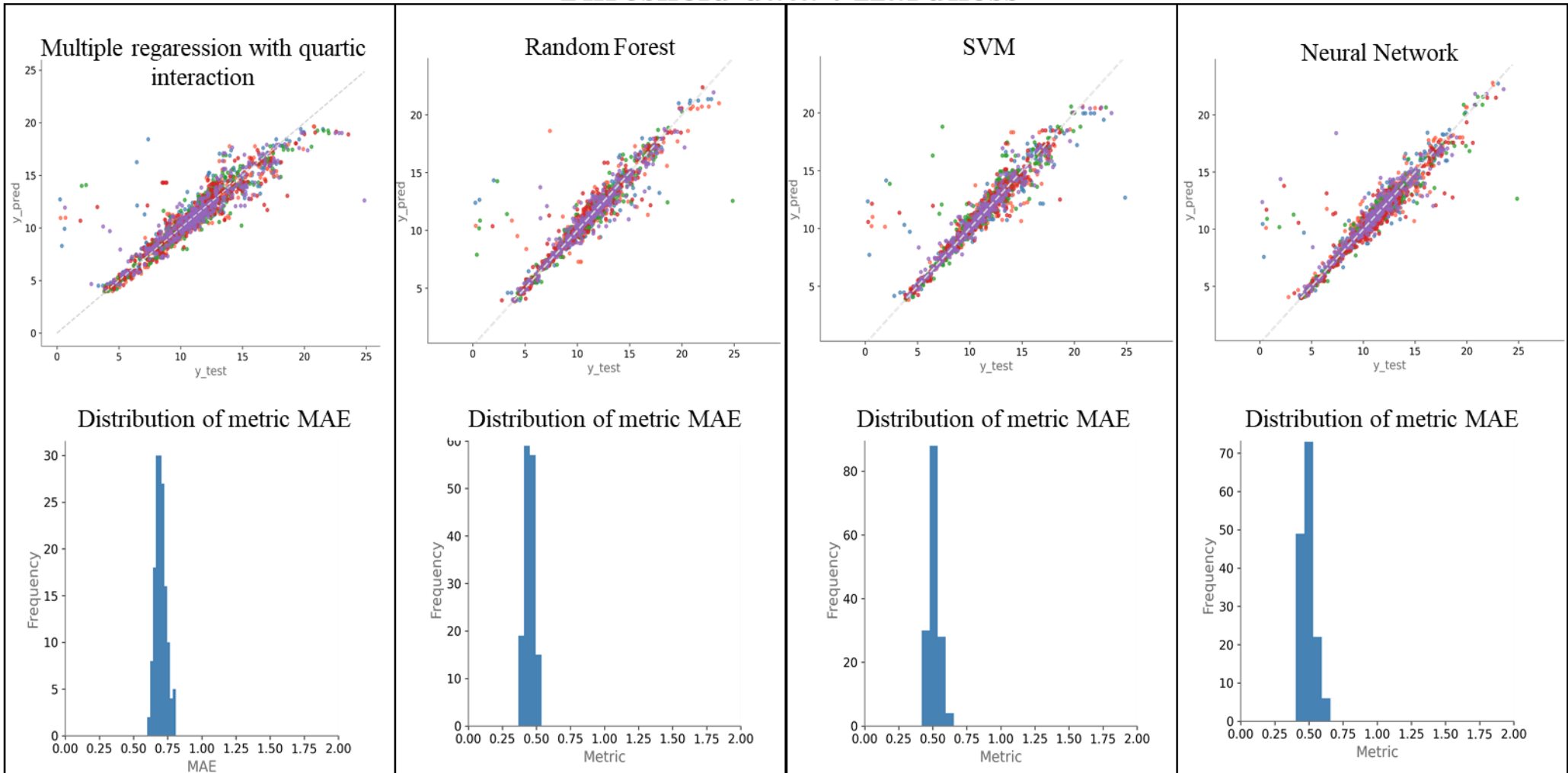
Supplementary Figure 32: Regressions between predicted and expected values on test sets of elastic modulus, and MAE metric distribution for different Machine Learning models, with "Averaged data" dataset

Raw data : Hardness



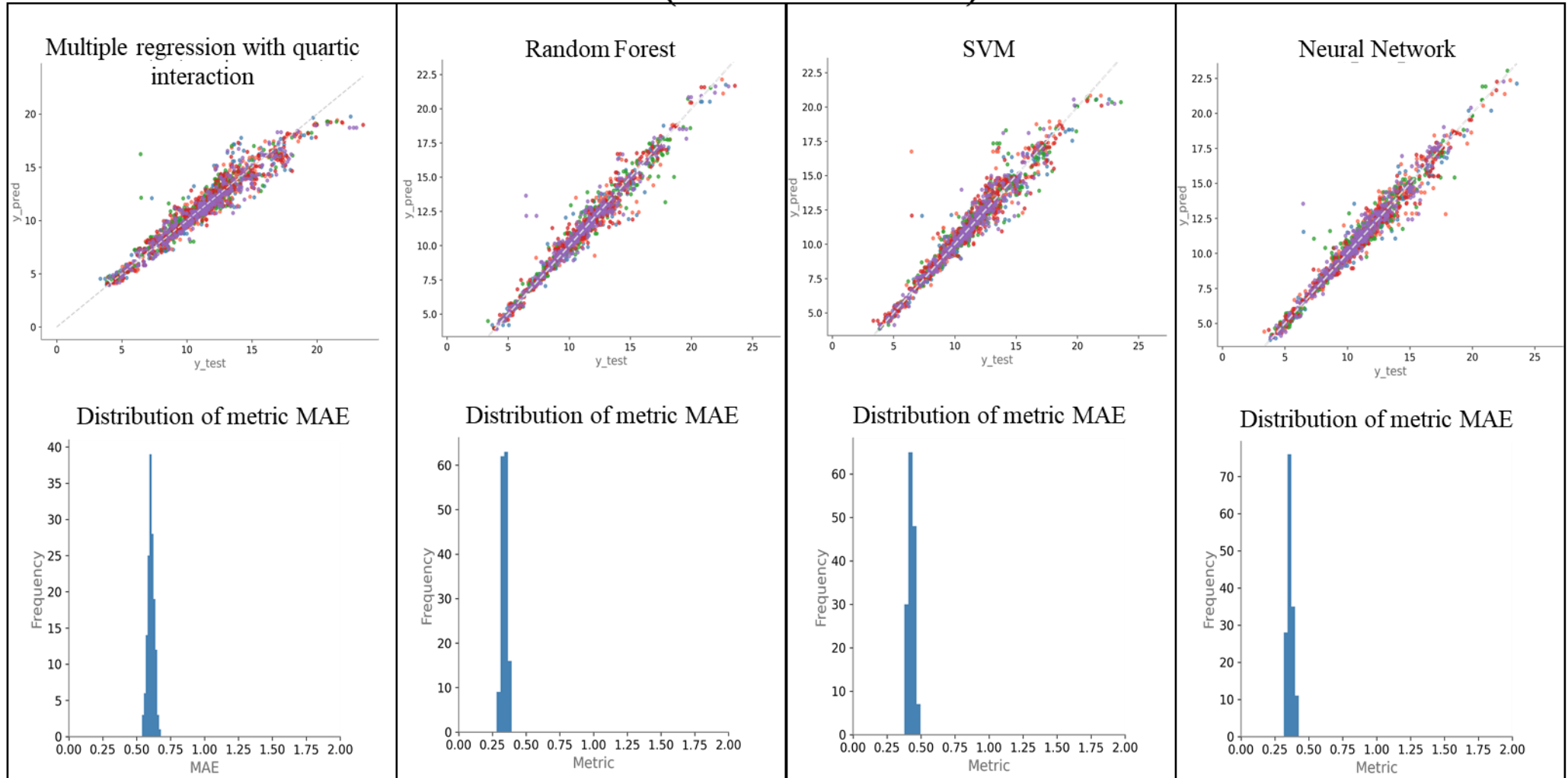
Supplementary Figure 33: Regressions between predicted and expected values on test sets of hardness, and MAE metric distribution for different Machine Learning models, with "Raw data" dataset

Threshold data : Hardness



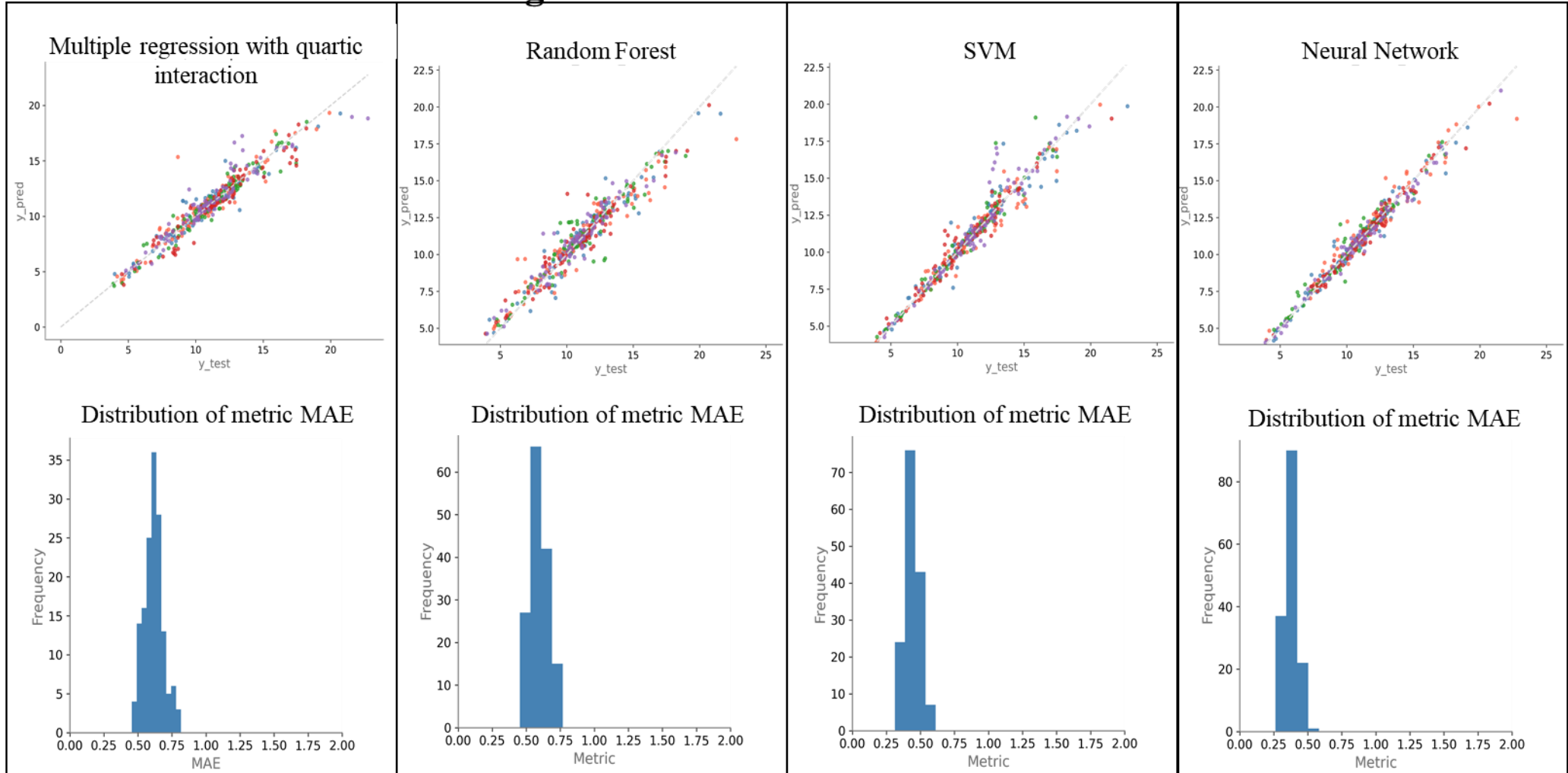
Supplementary Figure 34 : Regressions between predicted and expected values on test sets of hardness, and MAE metric distribution for different Machine Learning models, with "Threshold data" dataset

Processed data (outliers removed) : Hardness



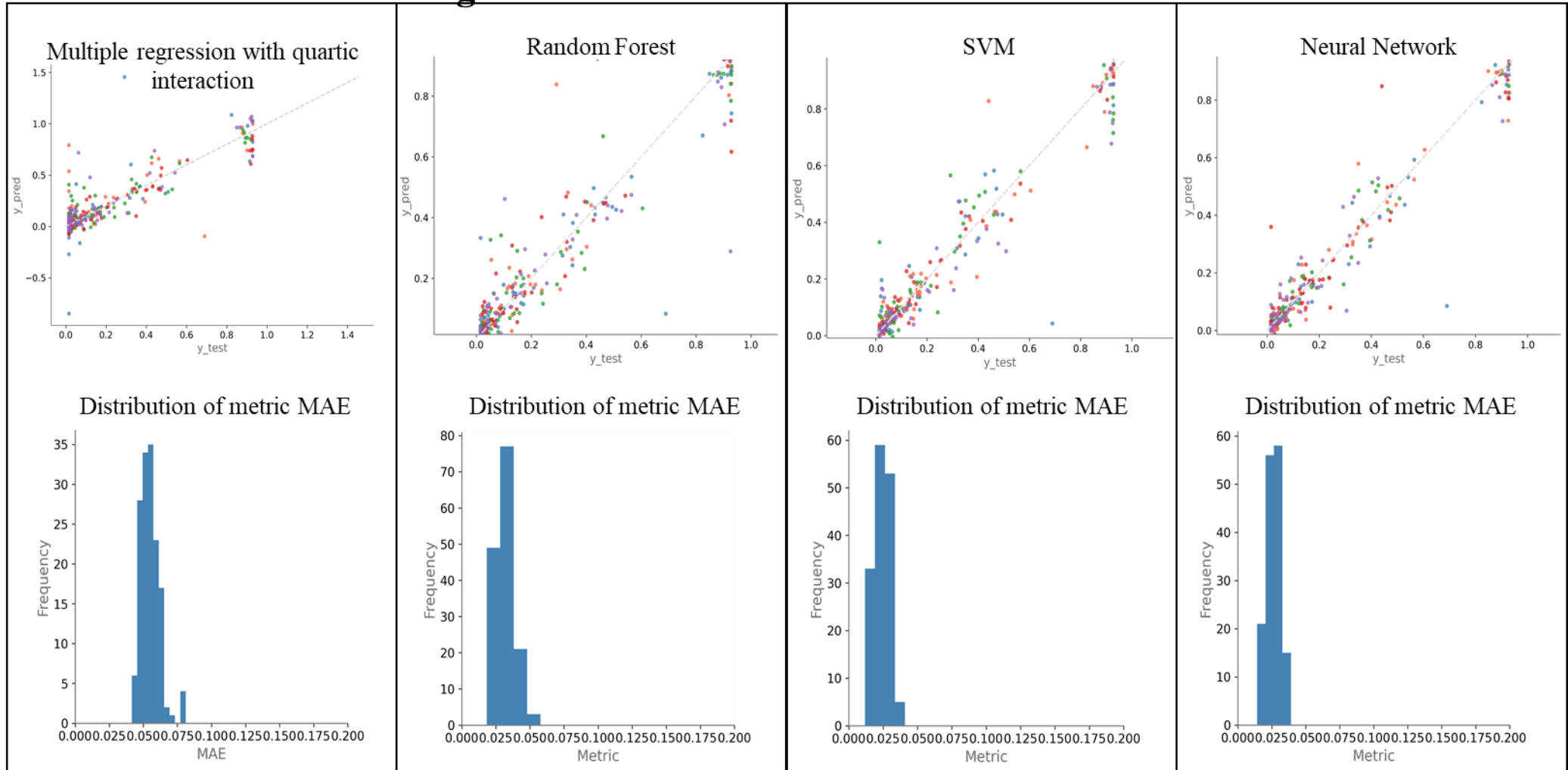
Supplementary Figure 35 : Regressions between predicted and expected values on test sets of hardness, and MAE metric distribution for different Machine Learning models, with "Statistically processed data" dataset

Averaged data without outliers : Hardness



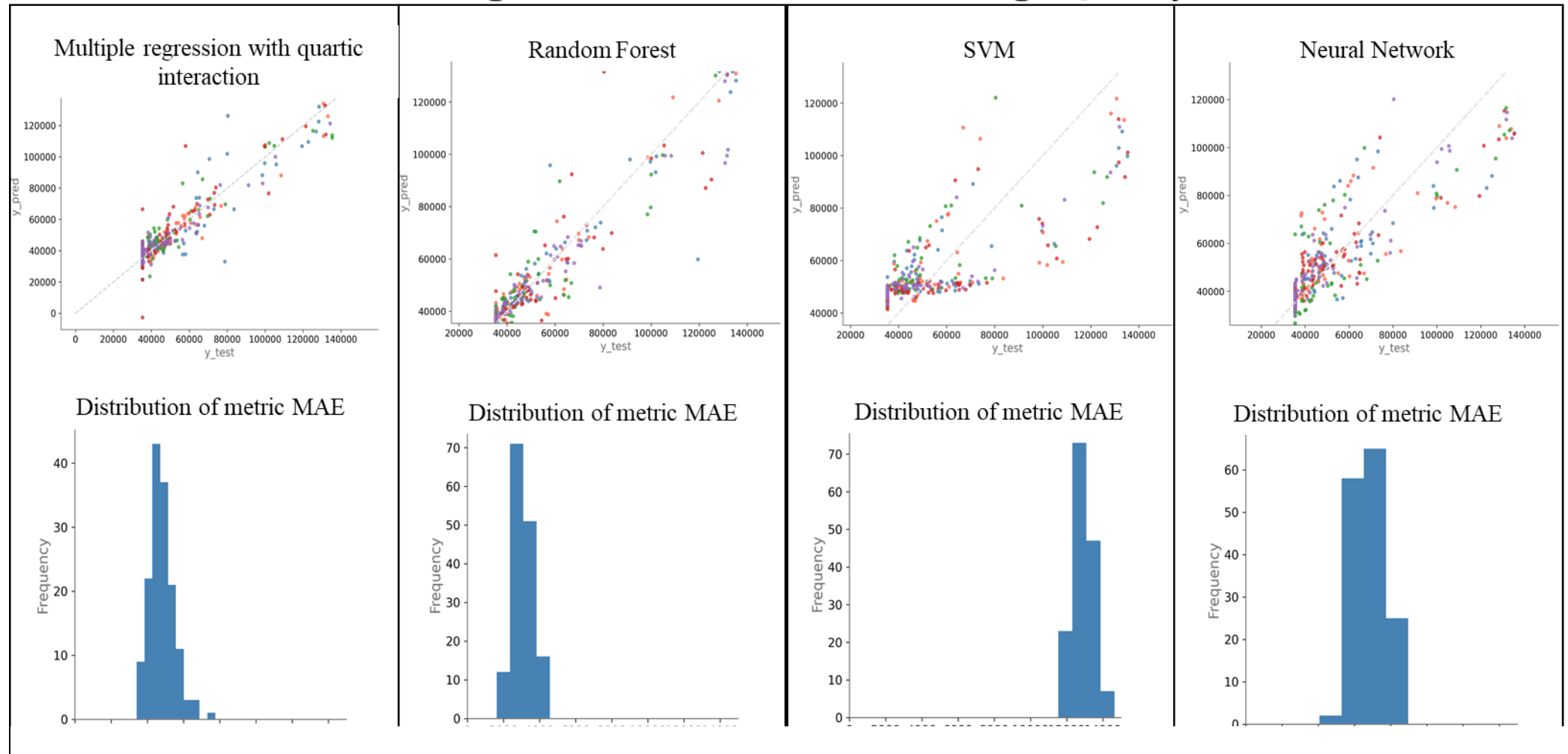
Supplementary Figure 36 : Regressions between predicted and expected values on test sets of hardness, and MAE metric distribution for different Machine Learning models, with "Averaged data" dataset

Averaged data without outliers : Confidence Index



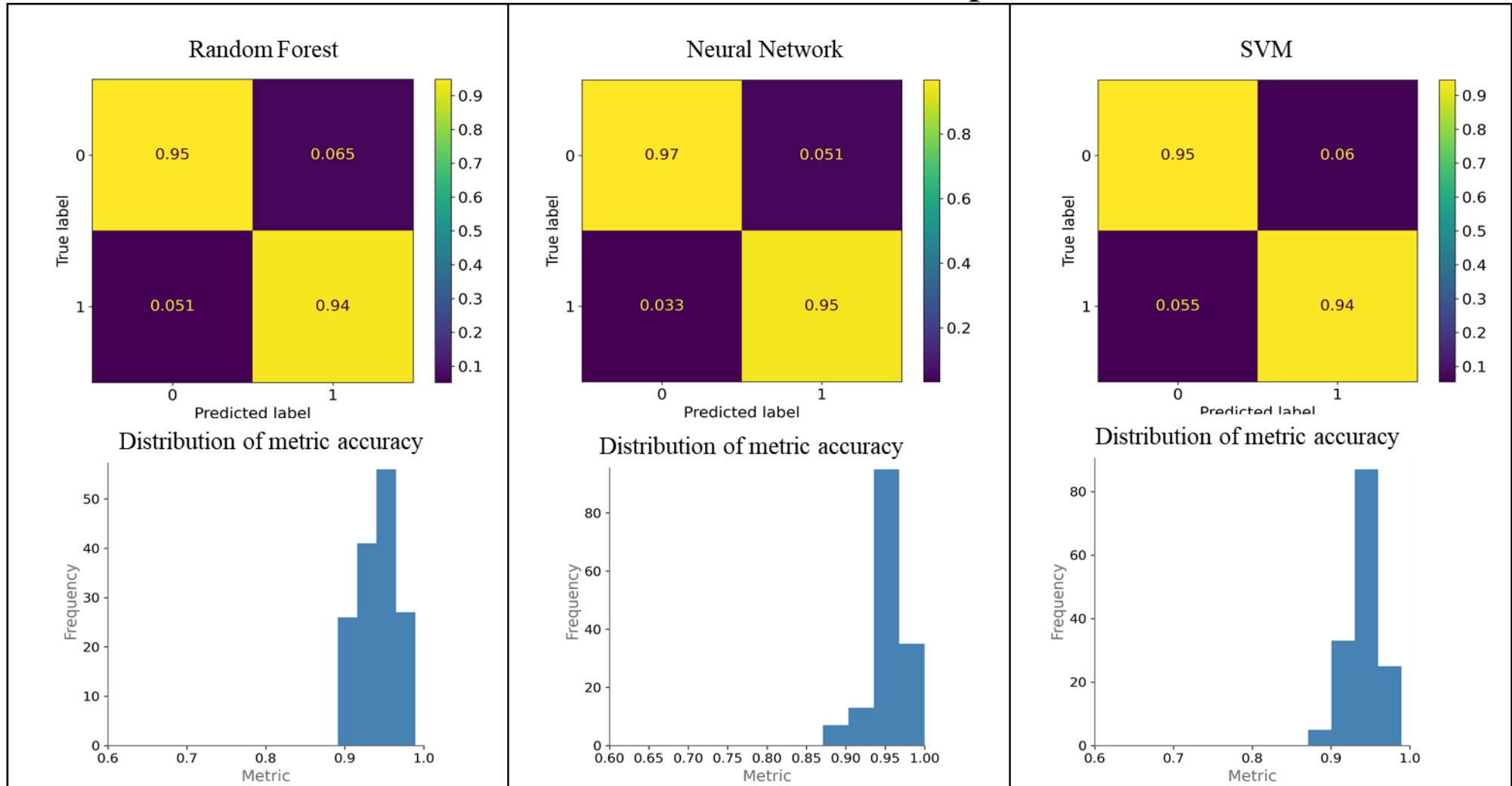
Supplementary Figure 37 : Regressions between predicted and expected values on test sets of EBSD Confidence Index (CI), and MAE metric distribution for different Machine Learning models, with "Averaged data" dataset

Averaged data without outliers : Image Quality



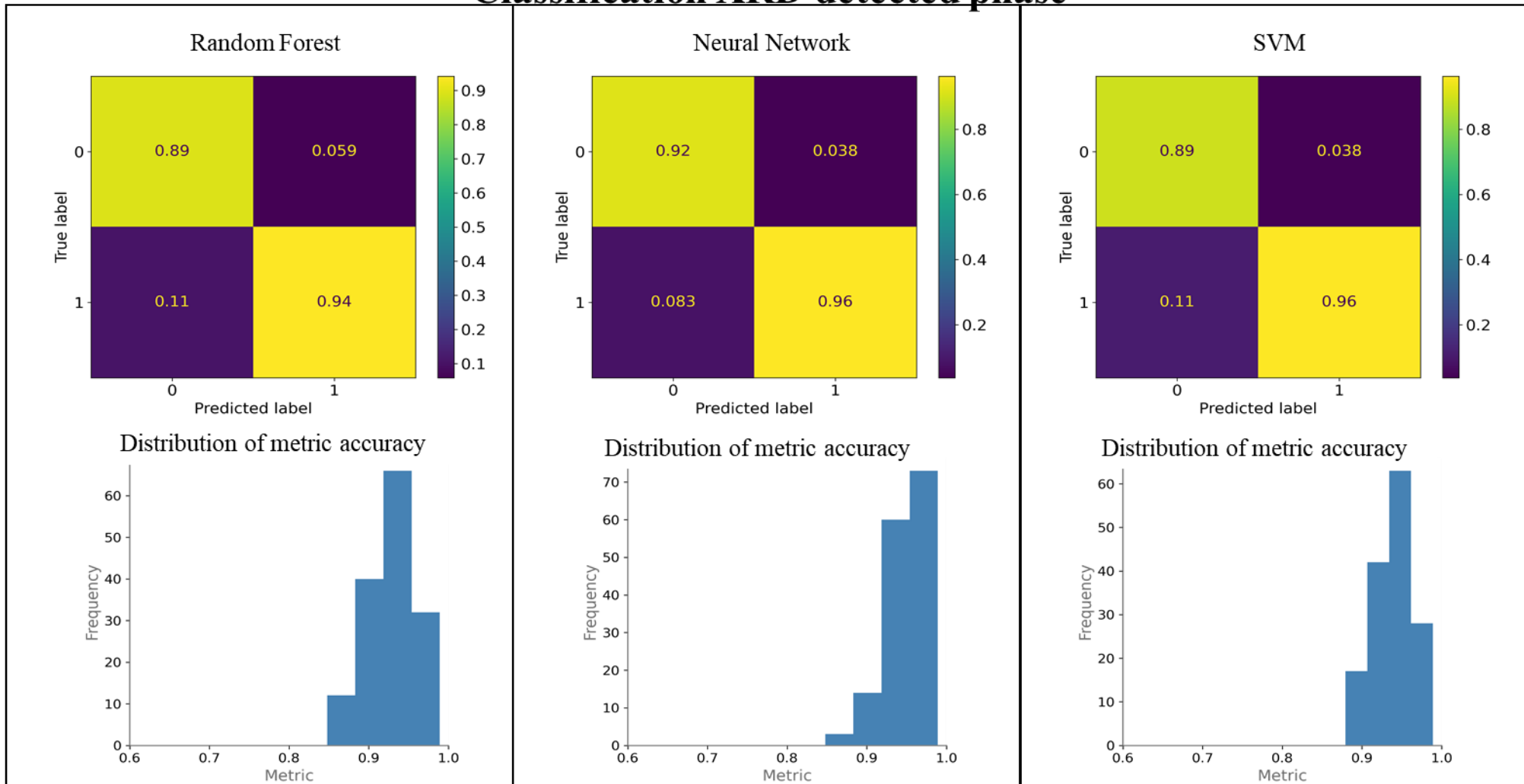
Supplementary Figure 38 : Regressions between predicted and expected values on test sets of EBSD Image Quality (IQ), and MAE metric distribution for different Machine Learning models, with "Averaged data" dataset

Classification EBSD detected phase

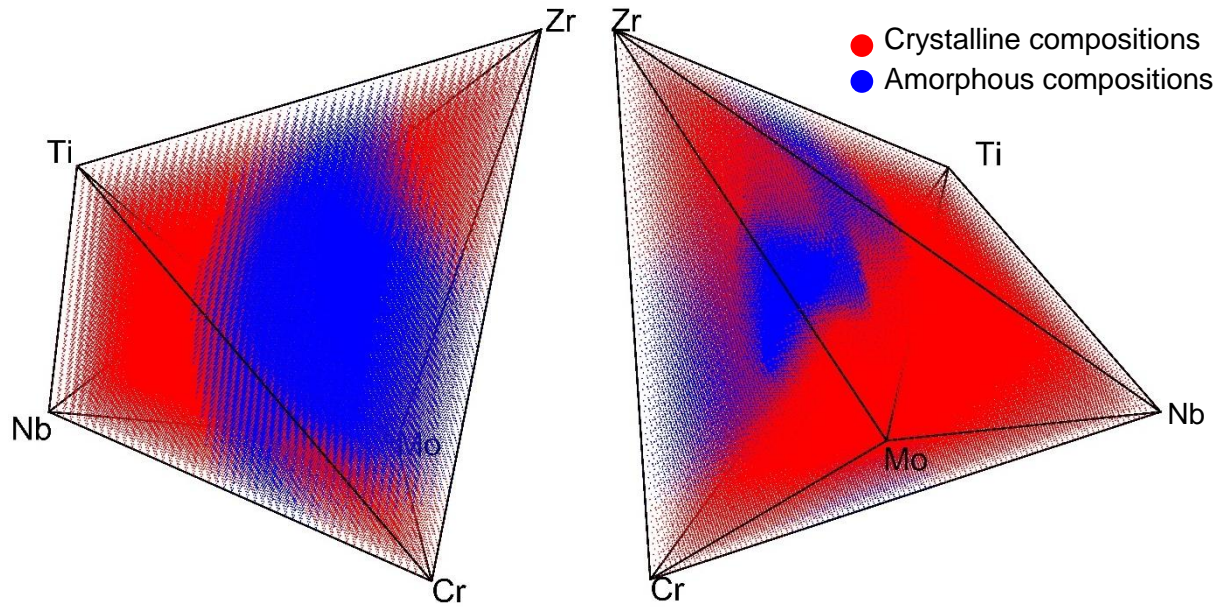


Supplementary Figure 39 : Confusion matrix between predicted and expected values on test sets of EBSD Confidence Index (CI), and accuracy metric distribution for different Machine Learning models, with "Averaged data" dataset

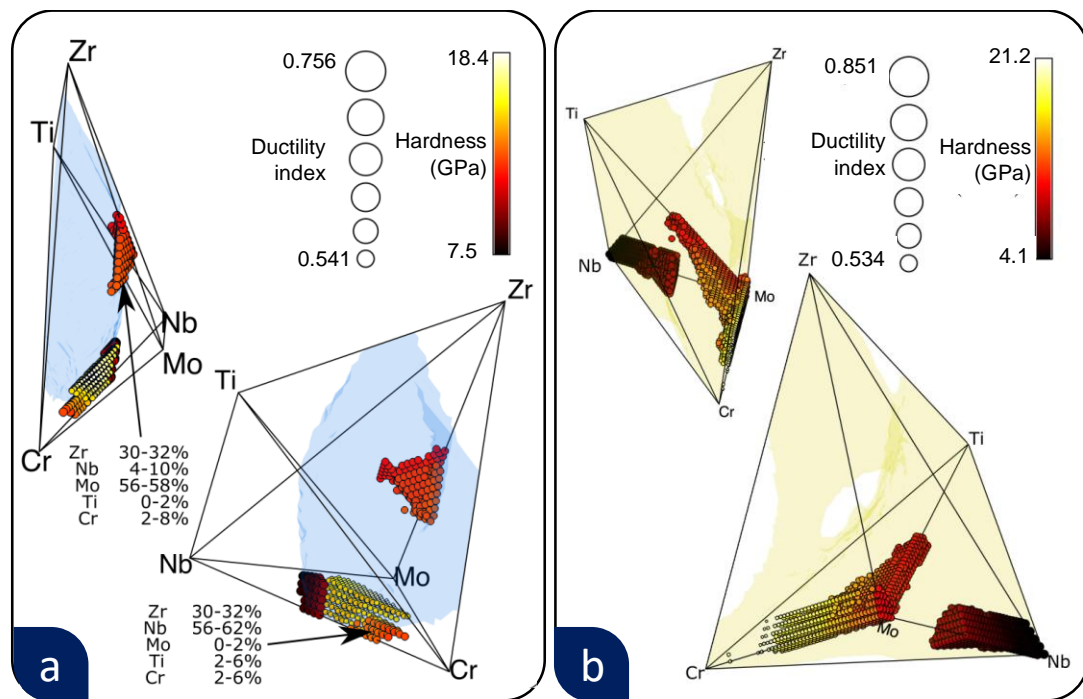
Classification XRD detected phase



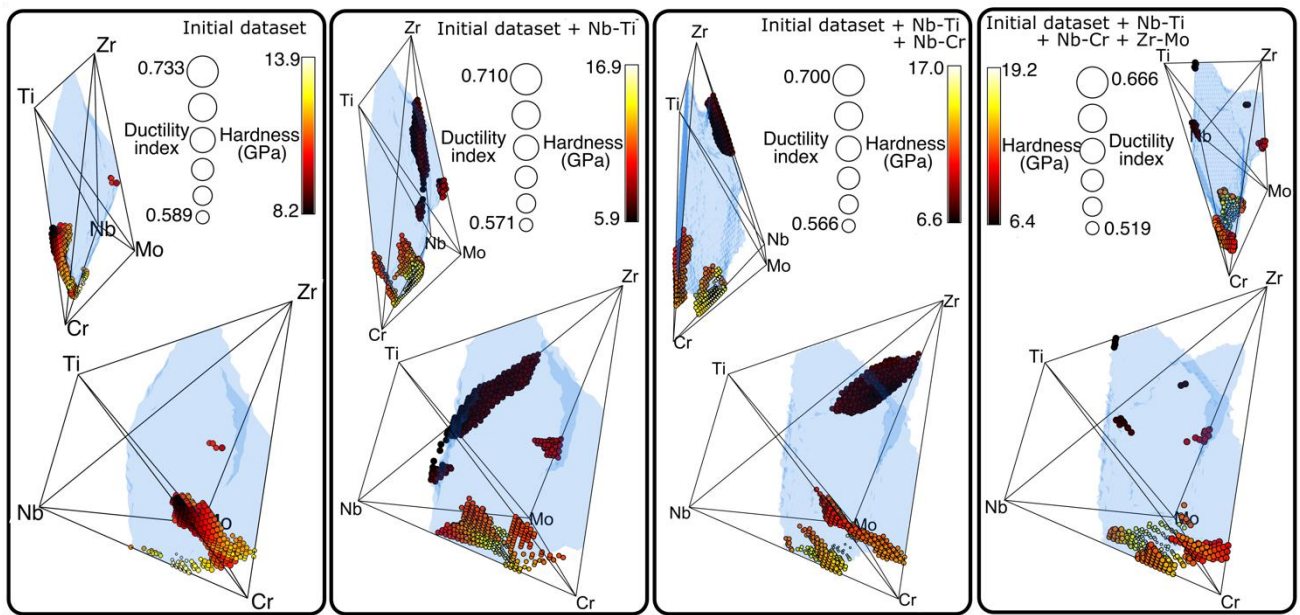
Supplementary Figure 40 : Confusion matrix between predicted and expected values on test sets of XRD phase classes, and accuracy metric distribution for different Machine Learning models, with "XRD classes" dataset



Supplementary Figure 41 : Predicted phases of the quinary system, with 2%at composition step for each element



Supplementary Figure 42 : Pareto-optimal composition obtained in amorphous (a) and crystalline (b) domains from Random Forest predictions



Supplementary Figure 43: Pareto-optimal compositions predicted by Random Forest models trained with intial dataset without outliers iteratively completed with binaries

Supplementary Tables

Supplementary Table 9: Adjusted R² mean and standard deviation with different Neural Network architectures

Model ID	Layers	Elastic modulus (GPa)		Hardness (GPa)		CI (EBSD)		IQ (EBSD)	
		R ² mean	R ² std	R ² mean	R ² std	R ² mean	R ² std	R ² mean	R ² std
keras-50x50	50x50	0.95155	0.00978	0.94553	0.01492	0.93036	0.04009	0.62771	0.06633
keras-100x100	100x100	0.95554	0.00996	0.95022	0.01443	0.93727	0.03869	0.65796	0.07495
keras-50x50x50	50x50x50	0.95590	0.01059	0.95420	0.01414	0.94019	0.03876	0.68137	0.06835
keras-100x100x100	100x100x100	0.96046	0.01025	0.95605	0.01490	0.94437	0.03407	0.69143	0.07255
keras-50x50x50x50	50x50x50x50	0.96118	0.01044	0.95597	0.01445	0.94471	0.03835	0.70412	0.06534
keras-100x100x100x100	100x100x100x100	0.96501	0.01096	0.95675	0.01502	0.94542	0.03687	0.74016	0.06794
keras-100x100x50x50	100x100x50x50	0.96233	0.01101	0.95621	0.01529	0.94542	0.03769	0.71875	0.05866
keras-50x100x100x50	50x100x100x50	0.96461	0.01112	0.95648	0.01492	0.94767	0.03496	0.71247	0.06614
keras-50x50x100x100	50x50x100x100	0.96397	0.01145	0.95621	0.01433	0.94623	0.03822	0.71301	0.07021

Supplementary Table 10: Adjusted R² mean and standard deviation with different Random Forest architectures

Model ID	nb estimators	min sample split	Elastic modulus (GPa)		Hardness (GPa)		CI (EBSD)		IQ (EBSD)	
			R ² mean	R ² std	R ² mean	R ² std	R ² mean	R ² std	R ² mean	R ² std
sklearn-rfr-50-5	50	5	0.96932	0.01162	0.95574	0.01520	0.89915	0.05425	0.91306	0.03812
sklearn-rfr-100-5	100	5	0.96867	0.01229	0.95534	0.01459	0.90349	0.05457	0.90781	0.04839
sklearn-rfr-150-5	150	5	0.96917	0.01189	0.95545	0.01413	0.90404	0.04565	0.90971	0.04744
sklearn-rfr-50-10	50	10	0.96844	0.01231	0.95612	0.01362	0.88974	0.05987	0.89536	0.04982
sklearn-rfr-100-10	100	10	0.97001	0.01113	0.95644	0.01391	0.89380	0.05562	0.89603	0.05803
sklearn-rfr-150-10	150	10	0.96966	0.01101	0.95673	0.01433	0.89240	0.06139	0.89722	0.05190
sklearn-rfr-50-20	50	20	0.96623	0.01185	0.95195	0.01383	0.82793	0.06857	0.79160	0.08317
sklearn-rfr-100-20	100	20	0.96672	0.01179	0.95182	0.01462	0.83050	0.06906	0.79278	0.09075
sklearn-rfr-150-20	150	20	0.96678	0.01194	0.95262	0.01434	0.83224	0.06657	0.79294	0.07834

Supplementary Table 11: Adjusted R² mean and standard deviation with different SVM architectures

Model ID	kernel	ε	C	Elastic modulus (GPa)		Hardness (GPa)		CI (EBSD)		IQ (EBSD)	
				R ² mean	R ² std	R ² mean	R ² std	R ² mean	R ² std	R ² mean	R ² std
sklearn-SVR-poly2-0.1-1	poly degree 2	0.1	1	0.64770	0.02415	0.45054	0.03960	0.52889	0.10465	0.48259	0.08805
sklearn-SVR-poly2-5-1	poly degree 2	5	1	0.65173	0.02363	0.34977	0.03093	-	-	0.47908	0.09120
sklearn-SVR-poly2-10-1	poly degree 2	10	1	0.65868	0.02298	-	-	-	-	0.47881	0.09840
sklearn-SVR-poly2-0.1-100	poly degree 2	0.1	100	0.68220	0.02861	0.45409	0.03907	0.53037	0.10289	0.55098	0.11257
sklearn-SVR-poly2-5-100	poly degree 2	5	100	0.68650	0.02602	0.34895	0.02883	-	-	0.56157	0.09704
sklearn-SVR-poly2-10-100	poly degree 2	10	100	0.69277	0.02761	-	-	-	-	0.55481	0.10237
sklearn-SVR-poly2-0.1-1000	poly degree 2	0.1	1000	0.68162	0.02691	0.45394	0.04012	0.52994	0.10231	0.56856	0.10993
sklearn-SVR-poly2-5-1000	poly degree 2	5	1000	0.68555	0.02731	0.34900	0.03067	-	-	0.56732	0.11718
sklearn-SVR-poly2-10-1000	poly degree 2	10	1000	0.69271	0.02366	-	-	-	-	0.56320	0.11465
sklearn-SVR-poly3-0.1-1	poly degree 3	0.1	1	0.78928	0.01989	0.73780	0.02115	0.66709	0.08985	0.53930	0.10503
sklearn-SVR-poly3-5-1	poly degree 3	5	1	0.79001	0.01878	0.56045	0.03899	-	-	0.53536	0.09841
sklearn-SVR-poly3-10-1	poly degree 3	10	1	0.78672	0.01927	-	-	-	-	0.53485	0.10345
sklearn-SVR-poly3-0.1-100	poly degree 3	0.1	100	0.84109	0.01798	0.73227	0.02508	0.65670	0.09307	0.60402	0.11137
sklearn-SVR-poly3-5-100	poly degree 3	5	100	0.84199	0.01612	0.46813	0.05576	-	-	0.59294	0.12660
sklearn-SVR-poly3-10-100	poly degree 3	10	100	0.84464	0.01585	-	-	-	-	0.60312	0.10706
sklearn-SVR-poly3-0.1-1000	poly degree 3	0.1	1000	0.84118	0.01429	0.73126	0.02513	0.65540	0.08740	0.62060	0.10772
sklearn-SVR-poly3-5-1000	poly degree 3	5	1000	0.84144	0.01590	0.45502	0.06433	-	-	0.61703	0.13163
sklearn-SVR-poly3-10-1000	poly degree 3	10	1000	0.84424	0.01594	-	-	-	-	0.62893	0.10856
sklearn-SVR-rbf-0.1-1	rbf	0.1	1	0.87155	0.01328	0.87339	0.01720	0.81380	0.05099	0.43320	0.05353
sklearn-SVR-rbf-5-1	rbf	5	1	0.87153	0.01423	0.68042	0.02872	-	-	0.43375	0.04176
sklearn-SVR-rbf-10-1	rbf	10	1	0.86993	0.01326	-	-	-	-	0.43254	0.04922
sklearn-SVR-rbf-0.1-100	rbf	0.1	100	0.94650	0.01033	0.93300	0.01417	0.86754	0.04463	0.45268	0.04545
sklearn-SVR-rbf-5-100	rbf	5	100	0.94758	0.00969	0.48717	0.06668	-	-	0.45297	0.05132
sklearn-SVR-rbf-10-100	rbf	10	100	0.94642	0.00978	-	-	-	-	0.45280	0.05170
sklearn-SVR-rbf-0.1-1000	rbf	0.1	1000	0.95586	0.00856	0.94547	0.01162	0.85543	0.06265	0.61782	0.07284
sklearn-SVR-rbf-5-1000	rbf	5	1000	0.95657	0.00957	0.39509	0.11648	-	-	0.61914	0.06816
sklearn-SVR-rbf-10-1000	rbf	10	1000	0.95646	0.00949	-	-	-	-	0.61714	0.06735
sklearn-SVR-sigmoid-0.1-1	sigmoid	0.1	1	0.23236	0.03093	0.00839	0.00660	0.21360	0.09643	0.37486	0.05532
sklearn-SVR-sigmoid-5-1	sigmoid	5	1	0.23877	0.03168	0.00509	0.00535	-	-	0.37602	0.05205
sklearn-SVR-sigmoid-10-1	sigmoid	10	1	0.25078	0.02898	-	-	-	-	0.37352	0.06160
sklearn-SVR-sigmoid-0.1-100	sigmoid	0.1	100	0.25278	0.03719	0.00051	0.00314	0.21786	0.10091	0.32782	0.05756
sklearn-SVR-sigmoid-5-100	sigmoid	5	100	0.25293	0.03961	0.00030	0.00269	-	-	0.32731	0.04887
sklearn-SVR-sigmoid-10-100	sigmoid	10	100	0.25227	0.03872	-	-	-	-	0.32624	0.05588
sklearn-SVR-sigmoid-0.1-1000	sigmoid	0.1	1000	0.25837	0.03243	0.00031	0.00277	0.22630	0.10271	0.00136	0.01602
sklearn-SVR-sigmoid-5-1000	sigmoid	5	1000	0.25870	0.04332	0.00029	0.00265	-	-	0.00097	0.01638
sklearn-SVR-sigmoid-10-1000	sigmoid	10	1000	0.25842	0.03589	-	-	-	-	0.00003	0.01556
sklearn-LinearSVR-0-1	linear	0	1	0.79768	0.01629	0.59932	0.02637	0.46505	0.07037	0.04937	0.03398
sklearn-LinearSVR-1-1	linear	1	1	0.79771	0.01396	0.60426	0.02885	-	-	0.05032	0.03722
sklearn-LinearSVR-10-1	linear	10	1	0.79817	0.01580	0.59890	0.02933	-	-	0.05055	0.03297
sklearn-LinearSVR-0-100	linear	0	100	0.79781	0.01493	0.59271	0.03201	0.27848	0.15148	0.29332	0.06368
sklearn-LinearSVR-1-100	linear	1	100	0.79814	0.01467	0.59804	0.02824	-	-	0.29328	0.06445
sklearn-LinearSVR-10-100	linear	10	100	0.79844	0.01739	0.60065	0.02923	-	-	0.29285	0.07184
sklearn-LinearSVR-0-1000	linear	0	1000	0.79588	0.01615	0.47895	0.10831	0.27531	0.14782	0.47240	0.05885
sklearn-LinearSVR-1-1000	linear	1	1000	0.79651	0.01700	0.54437	0.06450	-	-	0.47004	0.05889
sklearn-LinearSVR-10-1000	linear	10	1000	0.79714	0.01587	0.60108	0.02769	-	-	0.46907	0.06637
<hr/>											
	kernel	nu	C	R ² mean	R ² std	R ² mean	R ² std	R ² mean	R ² std	R ² mean	R ² std
sklearn-nuSVR-poly2-0.2-1	poly degree 2	0.2	1	0.64218	0.02257	0.47375	0.03086	0.55332	0.09297	0.53417	0.12033
sklearn-nuSVR-poly3-0.2-1	poly degree 3	0.2	1	0.73760	0.01780	0.73835	0.01805	0.64561	0.09264	0.57192	0.10640

sklearn-nuSVR-poly2-0.5-1	poly degree 2	0.5	1	0.66367	0.02054	0.47275	0.04037	0.48718	0.13222	0.55774	0.10597
sklearn-nuSVR-poly3-0.5-1	poly degree 3	0.5	1	0.78378	0.01657	0.74079	0.02227	0.65523	0.08251	0.56995	0.12838
sklearn-nuSVR-poly2-0.8-1	poly degree 2	0.8	1	0.65317	0.02475	0.45100	0.04063	0.47006	0.11219	0.55455	0.10465
sklearn-nuSVR-poly3-0.8-1	poly degree 3	0.8	1	0.79019	0.02116	0.73943	0.02361	0.62764	0.09301	0.58679	0.10497
sklearn-nuSVR-poly2-0.2-100	poly degree 2	0.2	100	0.70220	0.01986	0.47295	0.03052	0.55079	0.08690	0.53940	0.11195
sklearn-nuSVR-poly3-0.2-100	poly degree 3	0.2	100	0.84436	0.01404	0.73779	0.01882	0.63985	0.09999	0.58240	0.11333
sklearn-nuSVR-poly2-0.5-100	poly degree 2	0.5	100	0.70482	0.02263	0.47347	0.03576	0.49108	0.12945	0.55131	0.11015
sklearn-nuSVR-poly3-0.5-100	poly degree 3	0.5	100	0.84606	0.01334	0.74139	0.02162	0.66448	0.08575	0.58929	0.11595
sklearn-nuSVR-poly2-0.8-100	poly degree 2	0.8	100	0.68799	0.02461	0.45317	0.03995	0.46880	0.13334	0.56361	0.10338
sklearn-nuSVR-poly3-0.8-100	poly degree 3	0.8	100	0.84263	0.01474	0.73421	0.02226	0.62931	0.09633	0.59966	0.11580
sklearn-nuSVR-poly2-0.2-1000	poly degree 2	0.2	1000	0.70178	0.01812	0.47303	0.02860	0.55331	0.08037	0.55887	0.11809
sklearn-nuSVR-poly3-0.2-1000	poly degree 3	0.2	1000	0.84401	0.01324	0.73775	0.01936	0.63487	0.09860	0.64596	0.09807
sklearn-nuSVR-poly2-0.5-1000	poly degree 2	0.5	1000	0.70520	0.01982	0.47397	0.03752	0.48269	0.13319	0.56530	0.11261
sklearn-SVR-poly3-0.5-1000	poly degree 3	0.5	1000	0.84536	0.01567	0.74171	0.01646	0.65692	0.08829	0.63417	0.10603
sklearn-SVR-poly2-0.8-1000	poly degree 2	0.8	1000	0.68680	0.02359	0.45381	0.04379	0.47046	0.14326	0.57489	0.09677
sklearn-nuSVR-poly3-0.8-1000	poly degree 3	0.8	1000	0.84206	0.01524	0.73515	0.02236	0.62579	0.09766	0.62209	0.11886
sklearn-SVR-rbf-0.2-1	rbf	0.2	1	0.82898	0.01556	0.86064	0.01429	0.83021	0.04844	0.57130	0.08152
sklearn-nuSVR-rbf-0.5-1	rbf	0.5	1	0.86672	0.01296	0.87500	0.01538	0.85690	0.05348	0.52077	0.05938
sklearn-nuSVR-rbf-0.8-1	rbf	0.8	1	0.87172	0.01273	0.87332	0.01546	0.85197	0.05312	0.44577	0.04977
sklearn-nuSVR-rbf-0.2-100	rbf	0.2	100	0.94060	0.00896	0.93111	0.01328	0.93495	0.03516	0.56862	0.07519
sklearn-nuSVR-rbf-0.5-100	rbf	0.5	100	0.94765	0.00890	0.93471	0.01279	0.94043	0.03819	0.53582	0.06033
sklearn-nuSVR-rbf-0.8-100	rbf	0.8	100	0.94712	0.00960	0.93271	0.01488	0.94072	0.03617	0.47459	0.05070
sklearn-nuSVR-rbf-0.2-1000	rbf	0.2	1000	0.95369	0.00898	0.94425	0.01071	0.93640	0.04646	0.62634	0.07757
sklearn-nuSVR-rbf-0.5-1000	rbf	0.5	1000	0.95664	0.00987	0.94612	0.01179	0.93929	0.04526	0.62510	0.07224
sklearn-nuSVR-rbf-0.8-1000	rbf	0.8	1000	0.95619	0.00924	0.94498	0.01292	0.94031	0.04119	0.61607	0.07100

Supplementary Table 12: Adjusted R^2 mean and standard deviation with different Multiple Regressions with interactions

Model ID	Elastic modulus (GPa)		Hardness (GPa)		CI (EBSD)		IQ (EBSD)	
	R ² mean	R ² std	R ² mean	R ² std	R ² mean	R ² std	R ² mean	R ² std
Linear	0.79865	0.01447	0.60552	0.02666	0.47166	0.07028	0.47812	0.07008
Quadratic	0.89806	0.01112	0.77729	0.01773	0.66055	0.08076	0.67506	0.06994
Special Cubic	0.91323	0.01050	0.82796	0.01664	0.67995	0.07475	0.69844	0.06643
Cubic	0.93060	0.00967	0.86233	0.01701	0.75695	0.07196	0.76669	0.06997
Quartic	0.95065	0.01038	0.91586	0.01372	0.83266	0.07582	0.87080	0.05177

Supplementary Table 13: Accuracy (A), weighted averaged F1-score (F1w) and Hamming loss (HL) for different Neural

Model ID	Layers	EBSD phase class						DRX phase class					
		A mean	A std	F1w mean	F1w std	HL mean	HL std	A mean	A std	F1w mean	F1w std	HL mean	HL std
keras-50x50	50x50	0.95265	0.02279	0.95264	0.0228	0.04735	0.02279	0.94521	0.02885	0.94515	0.02905	0.05479	0.02885
keras-100x100	100x100	0.95245	0.02549	0.95242	0.02554	0.04755	0.02549	0.94564	0.02627	0.94559	0.02643	0.05436	0.02627
keras-50x50x50x50	50x50x50x50	0.95324	0.02312	0.95323	0.02314	0.04676	0.02312	0.94613	0.02971	0.94609	0.02988	0.05387	0.02971
keras-100x100x100	100x100x100	0.95533	0.02654	0.95531	0.02658	0.04467	0.02654	0.94758	0.02504	0.94753	0.02523	0.05242	0.02504
keras-50x50x50x50	50x50x50x50	0.95631	0.02289	0.95629	0.02291	0.04369	0.02289	0.94752	0.02479	0.94762	0.0247	0.05248	0.02479
keras-100x100x100x100	100x100x100x100	0.95624	0.02132	0.95622	0.02134	0.04376	0.02132	0.94673	0.02678	0.94666	0.02702	0.05327	0.02678
keras-100x100x50x50	100x100x50x50	0.95596	0.02273	0.95591	0.02277	0.04404	0.02273	0.94811	0.02676	0.94813	0.02673	0.05189	0.02676
keras-50x100x100x50	50x100x100x50	0.95631	0.02286	0.95628	0.02286	0.04369	0.02286	0.94717	0.02473	0.94714	0.02484	0.05283	0.02473
keras-50x50x100x100	50x50x100x100	0.95754	0.02378	0.95752	0.0238	0.04246	0.02378	0.95116	0.02572	0.95121	0.02577	0.04884	0.02572

Network classifier architectures

Supplementary Table 14: Accuracy (A), weighted averaged F1-score (F1w) and Hamming loss (HL) for different Random Forest classifier architectures

Model ID	nb estimators	min sample split	EBSD						DRX					
			A mean	A std	F1w mean	F1w std	HL mean	HL std	A mean	A std	F1w mean	F1w std	HL mean	HL std
sklearn-rfr-50-5	50	5	0.94009	0.02687	0.94008	0.02685	0.05991	0.02687	0.92461	0.02883	0.92433	0.02932	0.07539	0.02883
sklearn-rfr-100-5	100	5	0.94125	0.02546	0.94123	0.02548	0.05875	0.02546	0.92751	0.02643	0.92735	0.02667	0.07249	0.02643
sklearn-rfr-150-5	150	5	0.94131	0.0236	0.94128	0.02362	0.05869	0.0236	0.92738	0.02491	0.92727	0.02503	0.07262	0.02491
sklearn-rfr-50-10	50	10	0.93707	0.02535	0.93705	0.02535	0.06293	0.02535	0.91734	0.0303	0.91684	0.03086	0.08266	0.0303
sklearn-rfr-100-10	100	10	0.93851	0.02696	0.93848	0.02699	0.06149	0.02696	0.91617	0.03254	0.91572	0.03292	0.08383	0.03254
sklearn-rfr-150-10	150	10	0.9375	0.02382	0.93746	0.02385	0.0625	0.02382	0.91799	0.03062	0.91747	0.03126	0.08201	0.03062
sklearn-rfr-50-20	50	20	0.93038	0.02592	0.93035	0.02593	0.06962	0.02592	0.90217	0.03035	0.90053	0.03199	0.09783	0.03035
sklearn-rfr-100-20	100	20	0.93082	0.02739	0.93082	0.02738	0.06918	0.02739	0.90116	0.03145	0.89968	0.03255	0.09884	0.03145
sklearn-rfr-150-20	150	20	0.93333	0.02452	0.93328	0.02456	0.06667	0.02452	0.90061	0.03774	0.89903	0.039	0.09939	0.03774

Supplementary Table 15: Accuracy (A), weighted averaged F1-score (F1w) and Hamming loss (HL) for different SVM classifier architectures

Model ID	kernel	C	EBSD						DRX					
			A mean	A std	F1w mean	F1w std	HL mean	HL std	A mean	A std	F1w mean	F1w std	HL mean	HL std
sklearn-SVC-poly2-1	poly degree 2	1	0.79518	0.03948	0.79309	0.04028	0.20482	0.03948	0.75169	0.04112	0.75656	0.04009	0.24831	0.04112
sklearn-SVC-poly2-100	poly degree 2	100	0.81781	0.03628	0.81682	0.03641	0.18219	0.03628	0.78959	0.03891	0.79337	0.03758	0.21041	0.03891
sklearn-SVC-poly2-1000	poly degree 2	1000	0.81925	0.03532	0.81822	0.03567	0.18075	0.03532	0.78968	0.03928	0.7935	0.03861	0.21032	0.03928
sklearn-SVC-poly3-1	poly degree 3	1	0.87572	0.03142	0.87501	0.03195	0.12428	0.03142	0.809	0.0519	0.79633	0.06612	0.191	0.0519
sklearn-SVC-poly3-100	poly degree 3	100	0.9161	0.02456	0.91609	0.02456	0.0839	0.02456	0.86353	0.03313	0.86503	0.03235	0.13647	0.03313
sklearn-SVC-poly3-1000	poly degree 3	1000	0.9163	0.0269	0.91631	0.02686	0.0837	0.0269	0.865	0.03186	0.86711	0.03067	0.135	0.03186
sklearn-SVC-rbf-1	rbf	1	0.93555	0.02356	0.93553	0.02361	0.06445	0.02356	0.92599	0.02608	0.92662	0.02556	0.07401	0.02608
sklearn-SVC-rbf-100	rbf	100	0.94339	0.02353	0.94341	0.02351	0.05661	0.02353	0.93873	0.02156	0.9391	0.02123	0.06127	0.02156
sklearn-SVC-rbf-1000	rbf	1000	0.93555	0.02219	0.93553	0.02219	0.06445	0.02219	0.93574	0.02299	0.93617	0.02272	0.06426	0.02299
sklearn-SVC-sigmoid-1	sigmoid	1	0.65069	0.04392	0.65023	0.0442	0.34931	0.04392	0.50919	0.06349	0.50649	0.06721	0.49081	0.06349
sklearn-SVC-sigmoid-100	sigmoid	100	0.61939	0.04924	0.61881	0.04942	0.38061	0.04924	0.51179	0.06717	0.51047	0.06961	0.48821	0.06717
sklearn-SVC-sigmoid-1000	sigmoid	1000	0.62522	0.04406	0.62467	0.04428	0.37478	0.04406	0.49904	0.06617	0.49768	0.06758	0.50096	0.06617
sklearn-LinearSVC-1	linear	1	0.83183	0.03701	0.83163	0.03713	0.16817	0.03701	0.67802	0.04667	0.65457	0.05591	0.32198	0.04667
sklearn-LinearSVC-100	linear	100	0.82041	0.04196	0.8192	0.04258	0.17959	0.04196	0.66635	0.05226	0.65254	0.0598	0.33365	0.05226
sklearn-LinearSVC-1000	linear	1000	0.77381	0.06395	0.76824	0.06913	0.22619	0.06395	0.6232	0.08844	0.60472	0.10239	0.3768	0.08844

	kernel	nu	A mean	A std	F1w mean	F1w std	HL mean	HL std	A mean	A std	F1w mean	F1w std	HL mean	HL std
sklearn-nuSVC-poly2-0.2	poly degree 2	0,2	0.57124	0.14618	0.56709	0.14662	0.42876	0.14618	0.51071	0.10754	0.51999	0.10573	0.48929	0.10754
sklearn-nuSVC-poly3-0.2	poly degree 3	0,2	0.91386	0.02671	0.91382	0.02672	0.08614	0.02671	0.79249	0.09837	0.79234	0.09816	0.20751	0.09837
sklearn-nuSVC-poly2-0.5	poly degree 2	0,5	0.80244	0.03715	0.80067	0.03777	0.19756	0.03715	0.7716	0.04524	0.77567	0.04428	0.2284	0.04524
sklearn-nuSVC-poly3-0.5	poly degree 3	0,5	0.85927	0.04105	0.85785	0.04181	0.14073	0.04105	0.82313	0.06003	0.81369	0.07687	0.17687	0.06003
sklearn-nuSVC-poly2-0.8	poly degree 2	0,8	0.73962	0.0483	0.72988	0.05246	0.26038	0.0483	-	-	-	-	-	-
sklearn-nuSVC-poly3-0.8	poly degree 3	0,8	0.71621	0.07188	0.69504	0.08274	0.28379	0.07188	-	-	-	-	-	-
sklearn-nuSVC-rbf-0.2	rbf	0,2	0.93886	0.02149	0.93885	0.02151	0.06114	0.02149	0.93247	0.0258	0.93296	0.02549	0.06753	0.0258
sklearn-nuSVC-rbf-0.5	rbf	0,5	0.92248	0.02532	0.92248	0.02531	0.07752	0.02532	0.88063	0.03233	0.87997	0.0324	0.11937	0.03233
sklearn-nuSVC-rbf-0.8	rbf	0,8	0.89704	0.03197	0.89691	0.03207	0.10296	0.03197	-	-	-	-	-	-